Review

The Potential of Speleothems from Western Europe as Recorders of Regional Climate: A Critical Assessment of the SISAL Database

Franziska A. Lechleitner [1,*], **Sahar Amirnezhad-Mozhdehi** [2], **Andrea Columbu** [3], **Laia Comas-Bru** [2,4], **Inga Labuhn** [5], **Carlos Pérez-Mejías** [6] **and Kira Rehfeld** [7]

1   Department of Earth Sciences, University of Oxford, South Parks Road, Oxford OX1 3AN, UK
2   UCD School of Earth Sciences, University College Dublin, Belfield, Dublin 4, Ireland;
    sahar.amirnejad@gmail.com (S.A.-M.); l.comasbru@reading.ac.uk (L.C.-B.)
3   Department of Biological, Geological and Environmental Sciences, University of Bologna, Via Zamboni 67,
    40126 Bologna, Italy; andrea.columbu2@unibo.it
4   Centre for Past Climate Change and School of Archaeology, Geography & Environmental Sciences,
    Reading University, Whiteknights, Reading RG6 6AH, UK
5   Institute of Geography, University of Bremen, Celsiusstrasse 2, 28359 Bremen, Germany; labuhn@uni-bremen.de
6   Department of Geoenvironmental Processes and Global Change, Pyrenean Institute of Ecology (IPE–CSIC),
    Avda. Montañana 1005, 50059 Zaragoza, Spain; cperez@ipe.csic.es
7   Institute of Environmental Physics, Ruprecht-Karls-Universität Heidelberg, Im Neuenheimer Feld 229,
    69210 Heidelberg, Germany; krehfeld@iup.uni-heidelberg.de
*   Correspondence: franziska.lechleitner@earth.ox.ac.uk

check for updates

Abstract: Western Europe is the region with the highest density of published speleothem $\delta^{18}O$ ($\delta^{18}O_{spel}$) records worldwide. Here, we review these records in light of the recent publication of the Speleothem Isotopes Synthesis and AnaLysis (SISAL) database. We investigate how representative the spatial and temporal distribution of the available records is for climate in Western Europe and review potential sites and strategies for future studies. We show that spatial trends in precipitation $\delta^{18}O$ are mirrored in the speleothems, providing means to better constrain the factors influencing $\delta^{18}O_{spel}$ at a specific location. Coherent regional $\delta^{18}O_{spel}$ trends are found over stadial-interstadial transitions of the last glacial, especially in high altitude Alpine records, where this has been attributed to a strong temperature control of $\delta^{18}O_{spel}$. During the Holocene, regional trends are less clearly expressed, due to lower signal-to-noise ratios in $\delta^{18}O_{spel}$, but can potentially be extracted with the use of statistical methods. This first assessment highlights the potential of the European region for speleothem palaeoclimate reconstruction, while underpinning the importance of knowing local factors for a correct interpretation of $\delta^{18}O_{spel}$.

Keywords: SISAL database; speleothem; cave; oxygen isotopes; Western Europe; palaeoclimate

---

1. Introduction

Speleothems (secondary cave carbonates) are a widely used archive for the reconstruction of past terrestrial climate, and particularly for the investigation of high resolution climate variability, owing to their often exceptional chronological control [1,2]. The first version of the Speleothem Isotopes Synthesis

and AnaLysis (SISAL) database (SISAL_v1) contains 376 speleothem records from across the globe [3]. About a quarter of these records (92) are from Western Europe, making it the region with the highest density of published speleothem datasets worldwide [3]. This paper reviews these records within the wider (palaeo-)climatic context of Western Europe, with the objective to identify and promote the potential of cave sites in the region for future palaeoclimate studies. Moreover, we test the suitability of a large compilation of speleothem records to reveal the existence of regional trends in space and time [4].

While early studies on Western European speleothems principally focused on their availability for temperature reconstruction using $\delta^{18}O$ of the carbonate [5,6], it was quickly recognised that $\delta^{18}O_{spel}$ is driven by a complex interplay of regional and site-specific factors, such as moisture source and circulation dynamics, amount of precipitation, dripwater residence time in the overlying karst, cave temperature and ventilation dynamics, and potential kinetic effects during carbonate deposition [7,8]. Due to the filtering effect of the soil-karst system, the $\delta^{18}O_{spel}$ signal is usually strongly temporally attenuated compared to precipitation $\delta^{18}O$, and affected to varying degrees by local noise [4]. This is particularly pronounced at mid-latitude sites and over the Holocene, when ranges in $\delta^{18}O_{spel}$ are typically small (average standard deviation of Western European $\delta^{18}O_{spel}$ in SISAL_v1 is 0.36‰) and reflect only moderate climate shifts, as is apparent from other palaeoclimatic evidence (e.g., [9]). Over glacial-interglacial timescales, changes in the seasonality of precipitation and the spatial stationarity of climate patterns need to be considered as additional external drivers for variability in $\delta^{18}O_{spel}$ [10,11]. These, along with the fact that the signal-to-noise ratio with respect to underlying climatic variations of a given speleothem-based record depends on the local climate, geology, hydrology, and vegetation, underpins the importance of interpreting speleothem records in their specific context. Western Europe possesses the highest density of Global Network of Isotopes in Precipitation (GNIP; [12]) stations worldwide, which provide information on climatic drivers of precipitation $\delta^{18}O$ in the region. Moreover, many cave sites are well studied, with continuous, high-resolution multiannual cave monitoring time series, and a good understanding of local climatic conditions. Monitoring data from caves and their surface environment provide a basis for understanding speleothem growth conditions in a specific setting (e.g., [13–17]). These present-day observations are enormously useful to delineate and characterise processes influencing speleothem geochemistry, and of critical importance for the calibration of recent speleothem records against meteorological data.

Speleothems can provide precisely dated, high-resolution palaeoclimate records, and thus they are powerful archives for examining changes in climate variability and modes, and refine the picture obtained by other palaeoclimate archives. Focusing on Western Europe, where a large amount of palaeoclimate records from both speleothems and other archives is available, provides an opportunity to disentangle changes in mean climate state and variability.

Here, we provide an overview of climate in Western Europe, before describing the available data in SISAL_v1 [3]. This study is focused at highlighting the potential of this new database for reconstructing regional trends in $\delta^{18}O_{spel}$, as well as identifying common issues encountered with speleothem records from this region, in particular with respect to mixed climatic controls (temperature, moisture source, precipitation amount) that often affect Western European $\delta^{18}O_{spel}$.

2. Study Region and Climate

We define Western Europe roughly as the region between 11 and 16° E, and 36 and 71° N, based on political borders, and subdivide it into Southern Europe (<45° N; Iberian Peninsula, Southern France, Italy except the alpine region), Northern Europe (>45° N; Germany, Northern France, Belgium, Netherlands, Scandinavia), Great Britain and Ireland, and the Alpine region (Austria, Switzerland, Italian Alps; Figure 1; [18]). Soluble lithologies, notably carbonates and evaporites, are present throughout the region,

with the exception of most of Scandinavia, Northern Germany, the Netherlands, and parts of the Iberian Peninsula (Figure 1).
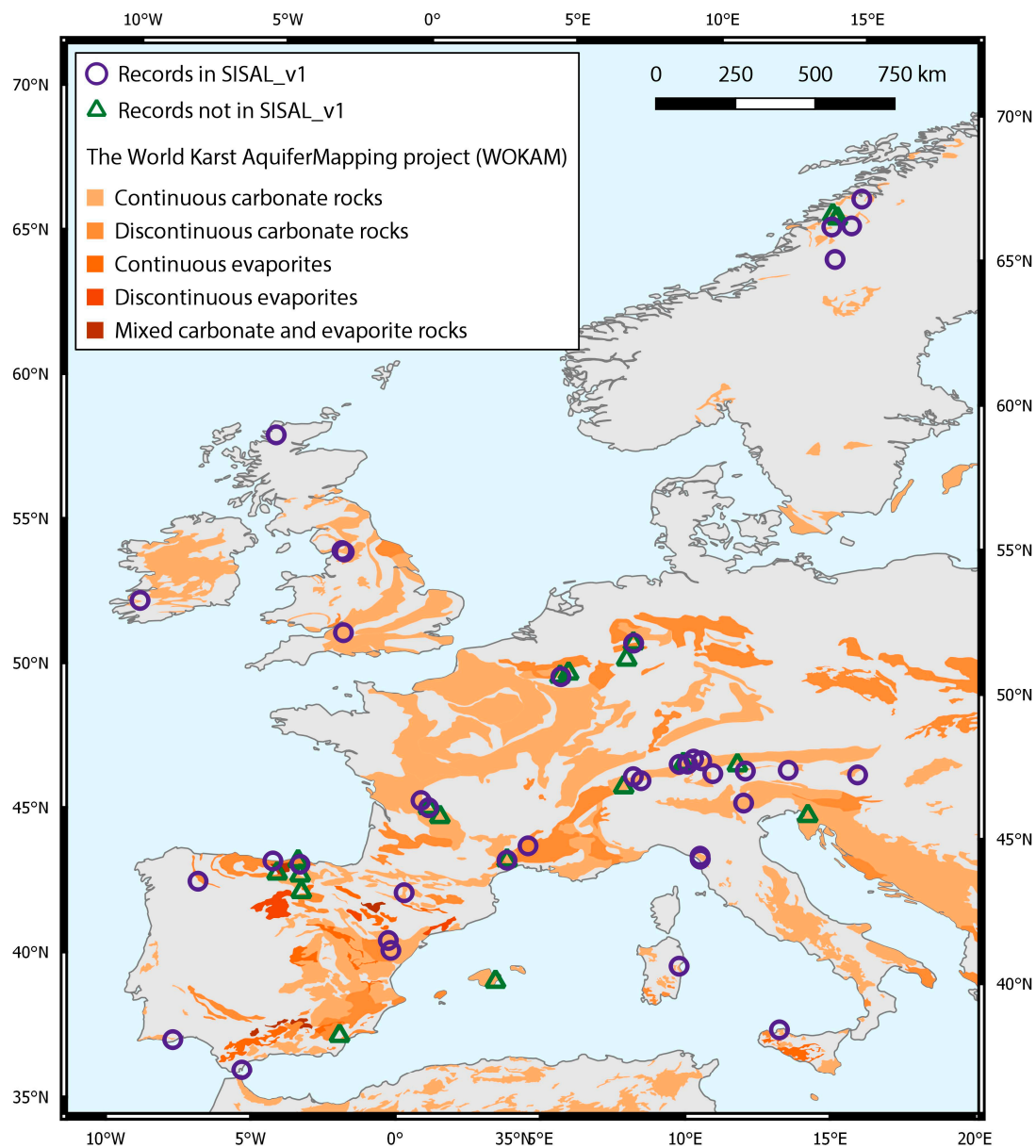

Figure 1. Map showing distribution of carbonate and evaporite rocks in Western Europe, provided by the World Karst Aquifer Mapping project (WOKAM; [19]). Purple circles show the sites included in SISAL_v1, while green triangles indicate study sites in the region identified by the Speleothem Isotopes Synthesis and AnaLysis (SISAL) working group, but not yet included in SISAL_v1 [20].

The present-day climate is characterised by strong spatial heterogeneity (Figure 2), and climate conditions become increasingly continental moving eastward from the Atlantic Ocean, as a result of predominant westerly moisture transport [21–23]. A latitudinal gradient is also present between the temperate-humid climate of Northern Europe and the seasonally arid climate of the Mediterranean region. These spatial gradients are reflected in the regional patterns of precipitation δ^{18}O, and are predominantly

related to the continental effect, with lower $\delta^{18}O$ due to progressive rainout and Rayleigh distillation with increasing distance from the Atlantic coast [4,24]. Deviations from this trend are found in Southern Europe, where the influence of water vapour from the Mediterranean Sea can lead to higher $\delta^{18}O$ values [25], and the Alpine region, where the altitude effect lowers precipitation $\delta^{18}O$ [24,26].

The most important driver of interannual climate variability is the North Atlantic Oscillation (NAO), which describes surface sea-level pressure differences between the Icelandic Low and the Azores High [27]. Variations in the NAO strongly influence winter surface temperatures, precipitation patterns, and storminess in the North Atlantic realm and in Western Europe [27–29], and modulate precipitation $\delta^{18}O$ [30–35]. On top of shifts in NAO polarity, changes in the location and geographical extension of the NAO's centres of action can occur, in particular related to the influence of other modes of climate variability in the North Atlantic region (e.g., the East Atlantic and Scandinavian patterns [36–38]). In the Mediterranean region, precipitation is largely controlled by the Western Mediterranean Oscillation (WeMO), understood as an East-West dipole of sea-level pressures between the Azores High and the Ligurian Low [39].
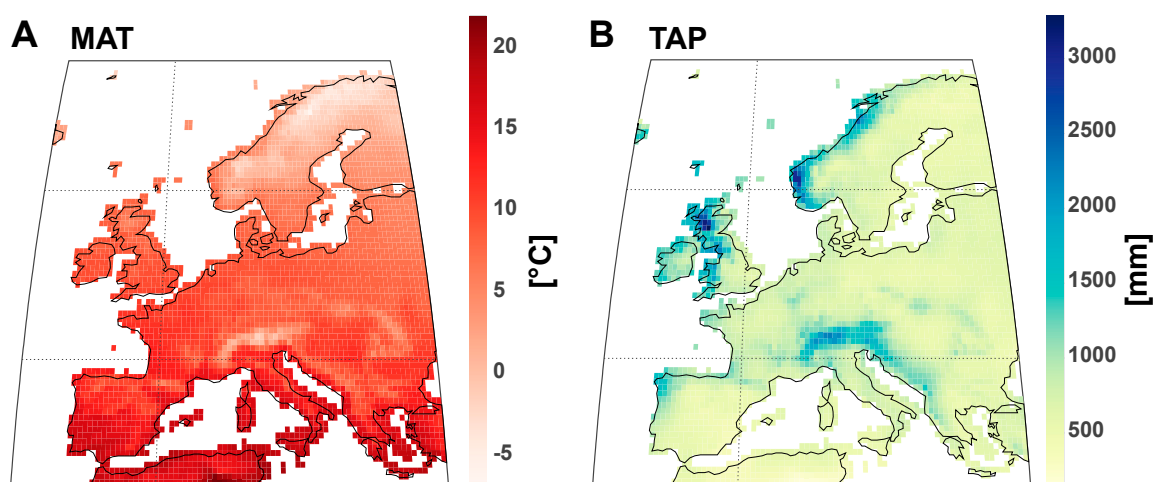

Figure 2. Map of the study region depicting mean annual surface air temperatures (MAT) (**A**) and total annual precipitation (TAP) (**B**) for the period 1958–2013, using the CRU-TS4.01 dataset [40]. The time period used was selected to match with the data extracted from the Global Network of Isotopes in Precipitation (GNIP; [12]) network and the SISAL_v1 records (see Figure 4).

Reconstructing regional and temporal variability in climate conditions through palaeoclimate records is challenging, as they are unevenly distributed in time and space and the accuracy of their chronologies varies widely across records. Thus, the potential of a large database of speleothem records lies in the possibility of extracting regional climate patterns from local responses at individual cave sites.

3. Western European Records in SISAL_v1

3.1. Spatio-Temporal Coverage and Regional Potential

In total, 146 published speleothem isotope records have been identified in Western Europe. Almost a hundred of these records (80 stalagmites, seven flowstones, and five composites) from 41 caves are currently included in SISAL_v1 [3], with 11 records from Great Britain and Ireland, 24 from Southern Europe, 22 from Northern Europe, and 35 from the Alpine region (Figure 1, Table 1).

Regional distribution of records with respect to the occurrence of soluble lithologies (carbonate and evaporite rocks) is patchy, in particular in central France and Germany, eastern central Spain,

and central-Southern Italy, where few records are published. While soluble lithologies do not necessarily contain caves and speleothems, as speleogenesis also depends on other factors, these regions are potential targets for future speleothem-based palaeoclimate investigations. However, many sites in the region are protected, either due to the rich speleothem decorations or the presence of archaeological and/or palaeontological remains, requiring minimal sampling impact and close collaboration with other researchers and local caving communities.

Temporal coverage of the Western European records in SISAL_v1 reaches back to ~400 ka, with stalagmite CC-1 from Antro del Corchia in Italy providing the longest record (~265 kyrs, i.e., kilo-years, including growth stops; [41]; Figure 3). Note that, in this study, ka BP is defined as thousand years before present, with the present referring to 1950 CE. The majority of the records however only cover the Holocene, with eight speleothems deposited during the last millennium (Figure 3B). Temporal coverage of speleothem records beyond the Holocene steadily decreases with increasing age, with 17% of all records starting to grow during the Last Glacial period (~12–80 ka), 15% during Marine Isotope Stage 5 (MIS 5; ~80–135 ka), and 10% before MIS 5. The average length of the records is ~16 kyrs, including growth interruptions (min: ~50 years; max: ~265 kyrs; median: ~6.7 kyrs). Many records (33%), especially the longest ones, contain at least one hiatus (Figure 3). The longest uninterrupted record, stalagmite CC-5 from Antro del Corchia, Italy, covers ~80 kyrs [42]. The average chronological resolution over all records is 17 years, gradually decreasing with record length/antiquity (Figure 2). The vast majority of records deposited since the end of the Last Glacial Maximum (LGM; 21 ka) have annual to multi-decadal resolution over most of their length (Figure 3B). Some records have seasonal (e.g., Gib04a from St. Michaels Cave, Gibraltar; [43]) or annual resolution (e.g., ER76 from Ernesto Cave, Italy; [44]), but others only provide multi-decadal and centennial information (e.g., CC-1 from Antro del Corchia, Italy; [41]). A tendency towards more speleothem growth during interstadials and interglacials is apparent, especially at high latitudes (Figure 3A), highlighting the dominance of temperature control on hydroclimate and vegetation/soil dynamics in this region.

Records not yet included in the SISAL database, due to difficulties in retrieving the original data [20], will improve the temporal coverage of the region. For example, records from Scandinavia covering past interglacials [45–47] will shed light on the temperature control of speleothem growth at high latitudes (Figure 2). Nevertheless, a bias towards more recent post-LGM reconstructions is apparent in our assessment of SISAL_v1, mainly because speleothems suffer from natural attrition [48]: recent deposits are usually more numerous as they are less likely to be lost and/or destroyed by processes such as floods, underground collapses, in-cave sedimentation covering the speleothems. Recent deposits also tend to be more suitable for geochemical analyses (e.g., less weathered and chemically altered) than older material. Additionally, there has been a strong interest of the community for very recent reconstructions that allow calibration with instrumental records, as this could pave the way toward quantitative reconstructions of past climatic variations (precipitation amount, temperature, etc.). Given the ability of speleothems to provide high resolution and very precisely dated records of past terrestrial climate, speleothem records from this region spanning further back in time have enormous potential, e.g., to better constrain conditions during past interglacials where climatic conditions were similar or warmer than today's [49]. This would be particularly useful for time periods beyond the range of radiocarbon dating (~50 ka), where chronological control in other archives becomes increasingly tenuous.
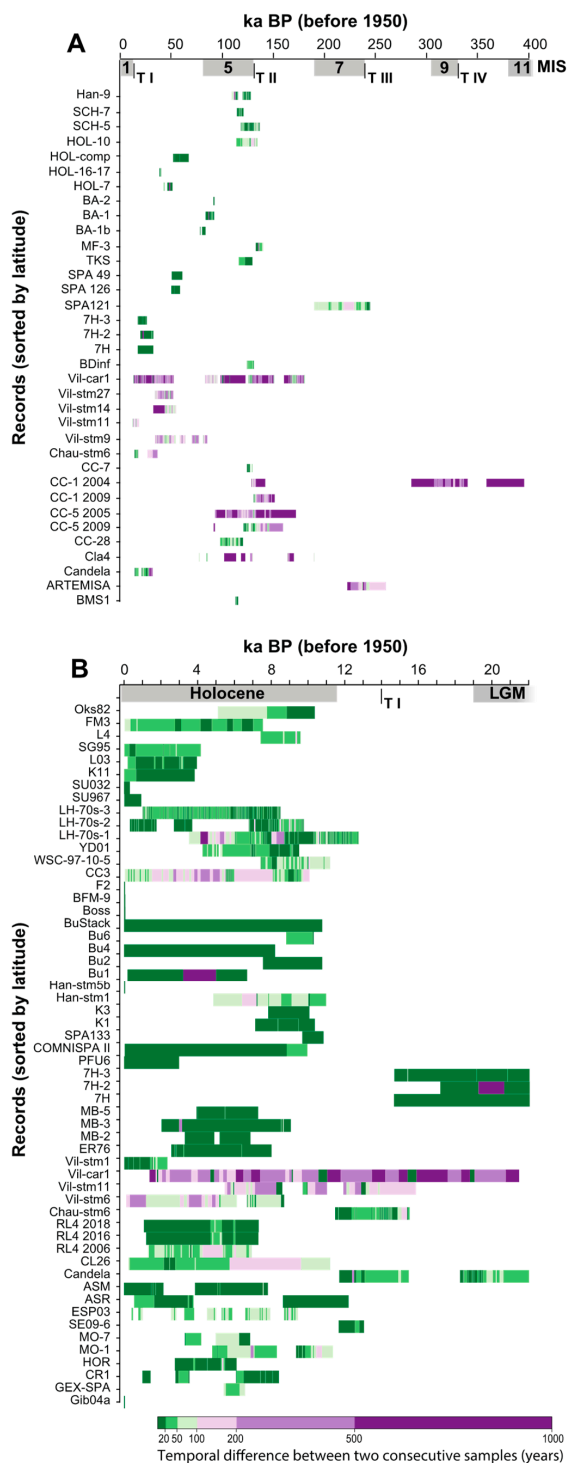
Figure 3. Temporal coverage of the Western Europe records included in SISAL_v1. (**A**) Records covering pre-Holocene time intervals. If a record extends into the Holocene, that part is shown in the next panel. (**B**) Records covering the last 22 ka. Marine Isotope Stage (MIS) and glacial terminations (T) timings according to Lisiecki and Raymo [50]. Hiatuses in individual records are shown by blank spaces. Records are sorted by latitude, with the northernmost site at the top.

Table 1. Summary of all records currently included in SISAL_v1 for Western Europe and records identified but not yet included (i.e., all records that do not have a SISAL entity_id). Information on records not included in SISAL_v1 was derived from the original publications. * no interpolated ages available.

site_name	*site_id*	Country	*Latitude* (N)	*Longitude* (E)	*entity_name*	*entity_id*	Min. Year (BP)	Max. Year (BP)	Reference
Antro del Corchia	145	Italy	43.98	10.22	CC-1_2004	313	125,432.63	393,407.69	[41]
Antro del Corchia	145	Italy	43.98	10.22	CC-5_2005	314	88,347	170,549.44	[42]
Antro del Corchia	145	Italy	43.98	10.22	CC-28	315	95,191.16	117,497.82	[51]
Antro del Corchia	145	Italy	43.98	10.22	CC-1_2009	316	127,997	148,970	[52]
Antro del Corchia	145	Italy	43.98	10.22	CC-5_2009	317	117,965	156,957	[52]
Antro del Corchia	145	Italy	43.98	10.22	CC-7	318	121,333	126,805	[52]
Antro del Corchia	145	Italy	43.98	10.22	COR-1				[53]
Antro del Corchia	145	Italy	43.98	10.22	CC-26		750	11,260	[54]
Atta		Germany	50.80	7.44	STAL-AH-1		1763	2723	[55]
Atta		Germany	50.80	7.44	AH-1		860	8430	[56]
B7		Germany	51.37	7.65	STAL-B7-1		6196	12,405	[57]
B7		Germany	51.37	7.65	STAL-B7-5		5850	8810	[57]
B7		Germany	51.37	7.65	STAL-B7-7		540	17,230	[57]
Baschg	15	Austria	47.25	9.67	BA-1b	70	75,492.44	80,896.94	[58]
Baschg	15	Austria	47.25	9.67	BA-1	71	80,982.06	89,489	[58]
Baschg	15	Austria	47.25	9.67	BA-2	72	88,609.98	89,723.31	[58]
Beatus		Switzerland	46.38	7.49	EXC-3		100,940	110,000	[58]
Beatus		Switzerland	46.38	7.49	EXC-4		77,450	107,080	[58]
Bourgeois Delaunay	73	France	45.67	0.51	BDinf	162	121,339	128,151	[59]
Brown's Folly mine	96	England	51.38	−2.37	Boss	192	−47	32	[60,61]
Brown's Folly mine	96	England	51.38	−2.37	BFM-9	193	−47	21	[60,61]
Brown's Folly mine	96	England	51.38	−2.37	F2	194	−46	13	[60,61]
Buca della Renella	133	Italy	44.08	10.21	RL4_2006	282	1215.56	6928.36	[62]
Buca della Renella	133	Italy	44.08	10.21	RL4_2016	283	1150.37	7262	[63]
Buca della Renella	133	Italy	44.08	10.21	RL4_2018	381	1024.11	7277.24	[64]
Bue Marino	97	Italy	40.25	9.62	BMS1	195	110,207	112,881	[65]
Bunker	117	Germany	51.37	7.66	Bu1	240	137	6644.9	[66]
Bunker	117	Germany	51.37	7.66	Bu2	241	7497.6	10,723.5	[66]
Bunker	117	Germany	51.37	7.66	Bu4	242	−57.3	8162.8	[66]
Bunker	117	Germany	51.37	7.66	Bu6	243	8749	10,258.2	[66]
Bunker	117	Germany	51.37	7.66	BuStack	244	−57.4	10,723.5	[66]
Chauvet	77	France	44.23	4.26	Chau-stm6	166	11,415	34,183	[67]
Clamouse	108	France	43.71	3.55	Cla4	211	74,460	187,405	[68]
Clamouse	108	France	43.71	3.55	CL26	212	142.33	11,178.79	[69]
Clamouse	108	France	43.71	3.55	Cla-stm5		432,000	611,000	[70]
Cova da Arcoia	143	Spain	42.61	−7.09	ESP03	310	340	9440	[71]
Cova de Cala Falco		Spain	39.5	3.3	CCF-03-03-01		48,000	112,000	[72]
Crag	98	Ireland	52.25	−9.43	CC3	196	−47	10,132	[69,73]
Cueva de Asiul	119	Spain	43.32	−3.59	ASR	248	488.61	12,160.96	[74]
Cueva de Asiul	119	Spain	43.32	−3.59	ASM	249	−62	7776.64	[74]
Cueva del Cobre		Spain	42.98	−4.37	C11		77	2614	[75]
Cueva Mayor		Spain	42.37	−3.51	SLX1		62	1513	[75]
Cueva Rosa		Spain	43.43	−5.13	Romeo		5294	8097	[76]
Ejulve	120	Spain	40.45	−0.35	ARTEMISA	251	218,975.67	257,426.49	[11]
Ejulve	120	Spain	40.45	−0.35	HOR	250	2708.44	6071.82	[77]
Entrische Kirche	121	Austria	47.16	13.15	TKS	252	113,389.5	126,889.04	[78]
Entrische Kirche	121	Austria	47.16	13.15	ENT-10		114,000	127,000	[78]
Excentrica	40	Portugal	37.10	−7.77	GEX-SPA	116	5329.36	6565.22	[79]
Gitana		Spain	37.44	−2.02	GC-01-05-02		58,000	274,000	[72]
Grotta di Carburangeli	129	Italy	38.17	13.16	CR1	277	947.73	8373.72	[80,81]

Table 1. *Cont.*

site_name	site_id	Country	Latitude (N)	Longitude (E)	entity_name	entity_id	Min. Year (BP)	Max. Year (BP)	Reference
Grotta di Ernesto	131	Italy	45.97	11.65	ER76	279	2511.48	7969.05	[44]
Grotta Savi		Italy	45.61	13.88	SV-1		1325	16,799	[82]
Hamarnes		Norway	66.42	14.02	Ham-85.2		4510	123,000	[45]
Han-sur-Lesse	16	Belgium	50.12	5.19	Han-stm1	73	4778	10,949	[83]
Han-sur-Lesse	16	Belgium	50.12	5.19	Han-stm5b	74	−44	16	[84]
Han-sur-Lesse	16	Belgium	50.12	5.19	Han-9	75	106,499.65	125,343.05	[85]
Han-sur-Lesse	16	Belgium	50.12	5.19	Proserpine		−51	471	[86]
Hölloch im Mahdtal	115	Austria	47.38	10.15	HOL-7	230	40,105	48,664	[87]
Hölloch im Mahdtal	115	Austria	47.38	10.15	HOL-16	231	36,701	63,546	[87]
Hölloch im Mahdtal	115	Austria	47.38	10.15	HOL-17	232	35,832	64,934	[87]
Hölloch im Mahdtal	115	Austria	47.38	10.15	HOL-18	233	52,509	57,283	[87]
Hölloch im Mahdtal	115	Austria	47.38	10.15	HOL-16-17	234	35,705	37,578	[87]
Hölloch im Mahdtal	115	Austria	47.38	10.15	HOL-comp	235	49,063	64,498	[87]
Hölloch im Mahdtal	115	Austria	47.38	10.15	HOL-10	236	110,844	131,765	[88]
Hölloch im Mahdtal	115	Austria	47.38	10.15	Stal-Hoel-1		1380	12,690	[89]
Hötting Breccia		Austria	47.28	11.39	HOT-1		73,900	98,700	[90]
Hötting Breccia		Austria	47.28	11.39	HOT-2		70,300	73,800	[90]
Hotton		Belgium	50.25	5.45			2750	11,150	[91]
Kaite		Spain	42.94	−3.57	comp.		394	9569	[92]
Kaite		Spain	42.94	−3.57	LV5		393	3885	[75]
Katerloch	100	Austria	47.08	15.55	K3	200	7786.62	10,027.08	[93]
Katerloch	100	Austria	47.08	15.55	K-2				[94]
Katerloch	100	Austria	47.08	15.55	K-4				[94]
Katerloch	100	Austria	47.08	15.55	K-5				[94]
Katerloch	100	Austria	47.08	15.55	K-7				[94]
Katerloch	100	Austria	47.08	15.55	K-8				[94]
Katerloch	100	Austria	47.08	15.55	K-RZ6-072007				[53]
Katerloch	100	Austria	47.08	15.55	K-Top3-Cl				[53]
Katerloch	100	Austria	47.08	15.55	K1	199	7079.5	10,324	[93]
Katerloch	100	Austria	47.08	15.55	K-6				[94]
Klapferloch	101	Austria	46.95	10.55	PFU6	201	−47	2943.04	[95]
Klapferloch	101	Austria	46.95	10.55	PFU-7				[95]
Klapferloch	101	Austria	46.95	10.55	PFU-8				[95]
Klapferloch	101	Austria	46.95	10.55	PFU-9				[95]
Klaus-Cramer		Austria	47.26	9.52	KC-1		54,560	71,940	[58]
Kleegruben	132	Austria	47.08	11.67	SPA_126	280	47,396	55,966	[96]
Kleegruben	132	Austria	47.08	11.67	SPA_49	281	47,816	58,266	[96]
Korallgrottan	102	Sweden	64.88	14.00	K11	202	−55	3791.88	[97]
Korallgrottan	102	Sweden	64.88	14.15	K1		6070	8629	[98]
La Faurie		France	45.13	1.18	Fra-stm-6				[53]
La Garma		Spain	43.43	−3.66	GAR-01		10,142	13,757	[99]
La Garma		Spain	43.43	−3.66	GAR-02				[100]
Labyrintgrottan	46	Sweden	66.06	14.68	L4	122	7347.5	9565.1	[98]
Lancaster Hole	8	England	54.22	−2.52	LH-70s-1	50	3456.22	12,717.56	[101]
Lancaster Hole	8	England	54.22	−2.52	LH-70s-2	51	261.86	9735.67	[102]
Lancaster Hole	8	England	54.22	−2.52	LH-70s-3	52	945.79	8462.88	[102]
Laphullet		Norway	66.31	14.18	PL-6		380,000	502,000	[47]
Larshullet	47	Norway	66.00	14.00	L03	123	130	3920.52	[103]
Milchbach	123	Switzerland	46.62	8.08	MB-2	255	3248.65	6830	[104]
Milchbach	123	Switzerland	46.62	8.08	MB-3	256	1986.95	9025.84	[104]
Milchbach	123	Switzerland	46.62	8.08	MB-6	258	*	*	[104]
Milchbach	123	Switzerland	46.62	8.08	MB-5	257	3889.71	7245.91	[104]

Table 1. *Cont.*

site_name	site_id	Country	Latitude (N)	Longitude (E)	entity_name	entity_id	Min. Year (BP)	Max. Year (BP)	Reference
Molinos	109	Spain	40.79	−0.45	MO-7	217	3253	6812	[77,105]
Molinos	109	Spain	40.79	−0.45	MO-1	216	4727	11,334.76	[77]
New St Michael's	89	Gibraltar	36.13	−5.35	Gib04a	182	−53.6	2	[43,106]
Okshola	26	Norway	67.00	15.00	FM3	95	−47	7515.2	[107]
Okshola	26	Norway	67.00	15.00	Oks82	96	5006	10,327.64	[107]
Pere Noel		Belgium	50.13	5.16	PN-stm-95-5		1800	12,900	[91,108]
Pindal	87	Spain	43.40	−4.53	Candela	180	11,640.32	29,339.98	[109,110]
Pippikin Pot	53	England	54.21	−2.51	YD01	129	4205.58	9478.94	[101,111]
Schafsloch	125	Switzerland	47.23	9.38	MF-3	260	130,050	137,390	[112]
Schneckenloch	105	Austria	47.43	9.87	SCH-5	206	115,340	134,085	[88]
Schneckenloch	105	Austria	47.43	9.87	SCH-7	207	111,588.73	118,314.57	[58]
Seso	106	Spain	42.46	0.04	SE09-6	208	11,616	12,995	[113]
Sieben Hengste	55	Switzerland	46.75	7.81	7H	133	14,620	29,873	[114]
Sieben Hengste	55	Switzerland	46.75	7.81	7H-3	135	14,639.45	23,536.89	[114]
Sieben Hengste	55	Switzerland	46.75	7.81	7H-2	134	17,137.17	29,940.32	[114]
Soylegrotta	57	Norway	66.00	14.00	SG95	137	−43	4141.22	[45]
Soylegrotta	57	Norway	66.00	14.00	SG92-4		4500	8000	[115]
Soylegrotta	57	Norway	66.00	14.00	SG-92-2		320,000	630,000	[46]
Soylegrotta	57	Norway	66.00	14.00	SG93		253	10,409	[6]
Spannagel	58	Austria	47.08	11.67	SPA12	138	60	5043	[116]
Spannagel	58	Austria	47.08	11.67	SPA70	139	4549	9894	[116]
Spannagel	58	Austria	47.08	11.67	SPA128	140	2520	6140	[116]
Spannagel	58	Austria	47.08	11.67	SPA127	141	2737	8449	[116]
Spannagel	58	Austria	47.08	11.67	COMNISPA II	142	−13	9930.6	[116]
Spannagel	58	Austria	47.08	11.67	SPA133	154	9636.5	10,796.1	[116]
Spannagel	58	Austria	47.08	11.67	SPA121	261	187,290	242,070	[117]
Spannagel	58	Austria	47.08	11.67	SPA-4		265,700	353,900	[118,119]
Spannagel	58	Austria	47.08	11.67	SPA-59		52,900	261,400	[120]
Spannagel	58	Austria	47.08	11.67	SPA-12		15	2040	[121]
Spannagel	58	Austria	47.08	11.67	SPA-119		220,500	226,900	[119]
Spannagel	58	Austria	47.08	11.67	SPA-52		91,100	204,100	[122]
Spannagel	58	Austria	47.08	11.67	SPA-11		117,000	202,800	[122]
Uamh an Tartair	21	Scotland	58.14	−4.93	SU967	85	−35	892	[123]
Uamh an Tartair	21	Scotland	58.14	−4.93	SU032	86	−53	271	[124]
Villars	4	France	45.43	0.78	Vil-stm6	27	−43	8657	[125]
Villars	4	France	45.43	0.78	Vil-stm9	28	31,437.91	82,854.5	[126,127]
Villars	4	France	45.43	0.78	Vil-stm11	29	5361	15,875	[67]
Villars	4	France	45.43	0.78	Vil-stm14	30	28,892.68	52,156.42	[127,128]
Villars	4	France	45.43	0.78	Vil-stm27	31	31,340.9	49,663.24	[126]
Villars	4	France	45.43	0.78	Vil-car1	32	1055	178,002	[129]
Villars	4	France	45.43	0.78	Vil#10B				[53]
Villars	4	France	45.43	0.78	Vil#1A				[53]
Villars	4	France	45.43	0.78	VilGal#1B				[53]
Villars	4	France	45.43	0.78	VilPlq-8				[53]
Villars	4	France	45.43	0.78	Vil-stm1	33	−38	2333	[130]
Villars	4	France	45.43	0.78	Vil-stm24		102,800	113,600	[70]
White Scar	66	England	54.17	−2.44	WSC-97-10-5	150	7347.87	11,190.74	[101,111]

3.2. Dating Methods and Chronologies

Any palaeoclimatic interpretation hinges on the accuracy and precision of the dating method and age modelling technique applied. Speleothems are known for their precise U-Th chronologies, but other dating methods (e.g., layer counting, radiocarbon) are applied as well, and methodologies are often combined. SISAL_v1 contains 1189 ages from Western European speleothems, 96% of which were obtained with the U-Th method. U-Th ratios were measured by Multi Collector-Inductively Coupled Plasma-Mass Spectrometry (MC-ICP-MS; 62% of the total) or Thermal Ionisation Mass Spectrometry (TIMS; 34% of the total). For the calculation of corrected ages, the most recent publications use the U-Th decay constants published in [131,132], while older datasets mostly refer to [133]. This is because decay constants have been updated over time as a result of increasing analytical precision and methodological developments. Although not having crucial implications on the final ages, it highlights the efforts for a better understanding of the U-Th systematics. Other dating approaches such as ^{14}C analyses (e.g., [43,130]), layer counting (e.g., [44,134]) or approaches combining multiple methods each represent ≤2% of the total. The median two sigma (2σ) uncertainty related to single ages is 1.2% (with respect to the final corrected ages), ranging between 0% and 131%; uncertainties of 0% refer only to the top of actively growing speleothems. The dating uncertainties vary according to the method used (Figure 4), with MC-ICP-MS dates being the most precise (median 0.9%; min 0.2%; max 131%), followed by TIMS (1.5%; 0.3%; 67%), layer counting (2%; 0%; 13%), combination of multiple approaches (4%; 1%; 7%) and ^{14}C (17%; 4%; 42%). It should be noted that U-Th uncertainty increases in younger samples (i.e., last millennia), reflecting the difficulties in measuring the low radiogenic ^{230}Th content for recent speleothems [135] (Figure 4). For these young speleothems, other dating methods such as ^{14}C and layer counting might be more suitable and result in less overall uncertainty, as demonstrated by Mattey et al. [43], who used a combination of ^{14}C measurements and counting of minima in seasonal stable carbon isotope ratio (δ^{13}C) cycles to derive a precise chronology for a 53-year old stalagmite (Gib04a) from Gibraltar. For laminae counting, uncertainties are usually attributed after a series of independent counts (e.g., [61]), and offsets between band-counted and radiometric ages might occur if annual layers are missing (undercounting) and/or if intra-annual lamination is present (overcounting; [136,137]).

A variety of methods and algorithms are available to convert single dates to an age-depth model and, in most cases, calculate the propagation of age uncertainties through time. For Western European speleothems in SISAL_v1, the modelling procedures used are: StalAge (25%; [138]), linear interpolation (19%), Bayesian (not including OxCal, Bacon, BChron, and COPRA; 11%), polynomial fit (10%), OxCal (3%; [139]) and others or a combination of methods (30%). Here, "combination of methods" usually stems from the use of different dating techniques, e.g., ^{14}C and laminae counting in Gib04a from Gibraltar [43] or U-Th analysis and laminae counting in speleothems in Uamh an Tartair [134] and Larshullet Cave [103]. In our dataset, 13% of all ages were excluded from the final age-depth models in the original publications, mostly because they were not in the correct stratigraphic order and were thus considered unreliable. In radiometric dating, out-of-sequence anomalous ages can occur due to diagenetic phenomena affecting the carbonate fabric, and/or sources of error during sample preparation and analysis (e.g., cross-contamination, environmental contamination, spike calibration problems; [65,140–143]).

All age modelling protocols have their advantages and shortcomings [144], and emphasise different aspects of chronology development. In many cases, the age model for a single speleothem needs to take into account specific properties of the sample, e.g., petrographic and geochemical anomalies, and is thus to a certain extent subjective to the decisions of the user. This is important to ascertain the quality of the age-depth model for an individual speleothem but might introduce biases. An updated age modelling technique intercomparison study appears timely with the publication of SISAL_v1 and would be helpful to determine common strengths and weaknesses in the models.
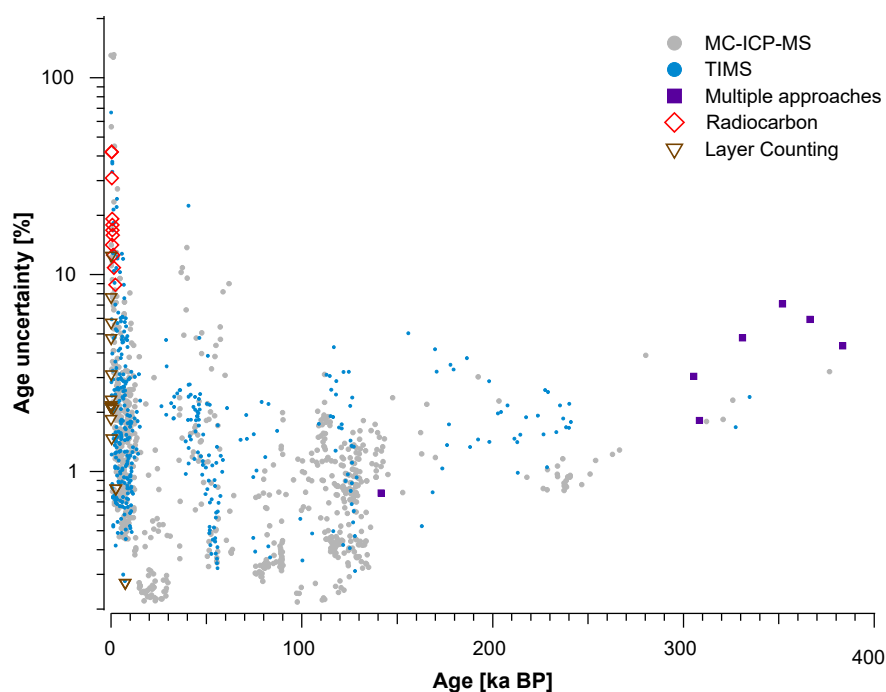
Figure 4. Dating methods, ages and age uncertainties. Shown are results in SISAL_v1 for Multi Collector-Inductively Coupled Plasma-Mass Spectrometry (MC-ICP-MS) and Thermal Ionisation Mass Spectrometry (TIMS) U-Th dating, ^{14}C dating, laminae counting, and combinations of these methods (mostly U-Th or ^{14}C combined with laminae counting). Note that, for simplicity, ages with 0% uncertainty (i.e., top of actively growing speleothems) were excluded.

3.3. Availability of Environmental and Monitoring Data

Local climate and cave monitoring data are useful for the characterisation of the karst system and the processes acting on geochemical signatures recorded in speleothems. With sufficiently long time series of outside and in-cave temperature, and isotopic composition of precipitation and drip water, it is possible to estimate the extent to which $\delta^{18}O_{spel}$ records are representative of present-day external environmental signals, i.e., temperature and precipitation $\delta^{18}O$. This is important, as fluid transfer through the karst system results in lagging, attenuation, or modification of the original precipitation signature. It must be noted, however, that this modern information needs to be carefully evaluated in the context of past climate, as the processes driving them might be temporally non-stationary and responding to climatic changes themselves (e.g., vegetation and soil cover, precipitation seasonality, changes in the temperature gradient between cave and exterior) or influenced by anthropogenic activities (e.g., land use changes, cave tourism, alteration of cave passages).

In Western Europe, temperature and precipitation data is widely available from meteorological stations for at least a few decades. Moreover, Europe has some of the longest meteorological records in the world, which go back to the 18th century (e.g., [145–147]). Gridded reanalysis or observational datasets provide continuous spatial coverage at high resolution since the late 19th century [40] and over 250 GNIP sites [12] provide monthly or event-based measurements of isotopes in precipitation, including the station with the longest record worldwide (Vienna-Hohe Warte, period covered: 1960–2016). Roughly 37% of these GNIP sites have been active for at least 10 years, and 63% for at least 5 years, providing an invaluable source of data to understand variability in precipitation and speleothem $\delta^{18}O$ (e.g., [148,149]). In-cave monitoring data, in contrast, is usually acquired within the context of specific speleothem studies

(e.g., [16,17,150]), and is thus often limited by short-term, project-based funding or limited accessibility to the cave. Of the 41 Western European cave systems included in the SISAL_v1 database, 22 have been monitored over at least one season (53% of all caves in SISAL_v1 of the region), as caves are often easily accessible, and more research funding is available than in some other regions.

3.4. Climate Controls on Speleothem Growth

In Western Europe, the response of speleothems to climate can generally be considered hierarchical, with growth presence/absence being the response to large climatic variations (glacial-interglacial changes), while millennial to seasonal variations are often recorded more specifically through geochemical variations. Speleothem growth is promoted during the warmer and more humid interglacials and interstadial periods (Figure 3A), aided by higher soil pCO_2 and the availability of infiltrating water. At high latitude/altitude locations, the most straightforward climatic influence on speleothem growth is the presence of ice or permafrost above the cave, which prevent fluid percolation through the soil-karst system. Presence/absence of growth and growth rate can thus both be powerful proxies for palaeoclimate conditions (e.g., [134,151,152]), with growth cessation and/or slow growth rates indicative of drier/colder stages, such as glacials and stadials (Figure 3A). This is observed at the Scandinavian cave sites, where speleothem growth is limited to interglacial time periods [47,107]. Conversely, evidence from high Alpine caves has shown that "subglacial" speleothem growth is possible if carbonate dissolution is promoted by sulphide oxidation, for instance seen in stalagmites from Milchbach and Sieben Hengste Caves, Switzerland [104,114] and Spannagel Cave, Austria [119].

Changing soil and vegetation activity is another mechanism influencing speleothem growth, as soil pCO_2 drives carbonate dissolution in the karst. Examples for such sites sensitive to changes in soil pCO_2 are Villars Cave in France, where cold phases during the last glacial are reflected by hiatuses in stalagmite Vil-stm9 [126], and Han-sur-Lesse Cave in Belgium, where stalagmite Han-9 stops growing after a period of drastic vegetation changes (shift to a more grass-dominated vegetation) and aridification synchronous with Greenland stadial 26 [85]. Milder stadial/glacial climate conditions at lower latitudes (e.g., Southern Italy and Southern Spain) appear to have allowed speleothem deposition at some sites [153], but so far these regions are poorly represented in the literature on interglacial-glacial transitions (Figure 1). Given the range of processes that can cause speleothem growth cessation, a climatic interpretation of growth presence/absence and growth rates hinges on an assessment of potential site-specific controls, e.g., drip pathway changes, tectonic activity, or anthropogenic influences. Growth presence/absence as a response to climatic change therefore needs to be ideally verified through replication with a number of samples from the same cave.

3.5. Controls on $\delta^{18}O_{spel}$

A multitude of factors can influence $\delta^{18}O_{spel}$, from local effects such as cave temperature and karst infiltration dynamics, to processes driving precipitation $\delta^{18}O$ (air temperature, precipitation amount and seasonality, moisture source and circulation dynamics). This is especially pronounced at the mid-latitude sites of Western Europe, where competing influences from several of these processes and a generally weaker climate control (especially during the Holocene) require detailed evaluation of the drivers of $\delta^{18}O_{spel}$.

The $\delta^{18}O_{spel}$ at sites included in SISAL_v1 is interpreted as dominantly reflecting air temperature (17 sites), precipitation amount (six sites), moisture source (one site), or a mixed signal of temperature and amount/moisture source (nine sites). The interpretation of $\delta^{18}O_{spel}$ remains unclear for eight sites, as the original publications had a different focus.

A dominant temperature signal is found principally at high-altitude sites in the Alps (Baschg [58], Entrische Kirche [78], Grotta di Ernesto [44], Hölloch im Mahdtal [87], Katerloch [93], Kleegruben [96], Schafsloch [112], Schneckenloch [58,88], Sieben Hengste [114]). At these sites, $\delta^{18}O_{spel}$ is understood to closely reflect precipitation $\delta^{18}O$, which is highly correlated to changes in air temperature during moisture condensation, with higher (lower) $\delta^{18}O$ reflecting warmer (colder) conditions (e.g., [87]). The authors of the original studies however emphasise that factors such as rainfall seasonality [58,78,93,112] or moisture source changes [87,88,117] play an additional role in the modulation of $\delta^{18}O_{spel}$, preventing a quantitative reconstruction of surface air temperatures. Interestingly, an opposite $\delta^{18}O$-temperature relationship (higher $\delta^{18}O_{spel}$ corresponding to lower temperature) has been reported for some alpine sites, most prominently for the Holocene portion of the Spannagel Cave record, where $\delta^{18}O_{spel}$ has been interpreted in terms of variable dripwater sources (snowmelt water vs. rainfall), with more negative $\delta^{18}O$ values reflecting a larger contribution of melt waters and less negative $\delta^{18}O$ explained by a stronger share of meteoric waters due to glacier retreat during interglacials [120,122]. The high-latitude Scandinavian caves (Søylegrotta [45], Okshola [107], Labyrintgrottan [98], Korallgrottan [97] and Larshullet [103]) show the same reversed $\delta^{18}O$-temperature relationship, corroborated by temperature calibration studies [6,45], and are also explained by seasonally selective infiltration during snowmelt [98,107]. Only three sites at lower altitudes report a dominant temperature effect on $\delta^{18}O_{spel}$ (Han-sur-Lesse [85], Clamouse [68,69], and Crag [69]).

Sites with a dominant influence of precipitation amount on $\delta^{18}O_{spel}$ are widely spread throughout the region (Antro del Corchia [41,42,51,52], Buca della Renella [62,63], Bue Marino [65], Burgeois-Delaunay [59], Cueva de Asiul [74], Klapferloch [95]). In all these cases, higher (lower) $\delta^{18}O_{spel}$ is interpreted to reflect lower (higher) rainfall amount, as a consequence of isotopic depletion of precipitation during large storms [154]. Correlating speleothem $\delta^{18}O$ and carbon isotope ratios ($\delta^{13}C$) often helps discerning whether $\delta^{18}O_{spel}$ is driven by precipitation amount, as enhanced rainfall intensifies soil activity and increase the drip rate, resulting in lower speleothem $\delta^{13}C$ (e.g., [59,65]).

Several sites (Bunker [66], Cova da Arcoia [71], El Pindal [109], Grotta di Carburangeli [80], Molinos [77], Uamh an Tartair [123,124], Villars [67,126–129]) show a mixed signal of temperature and precipitation amount controls, which complicates their interpretation.

Moisture source is the third main driver for $\delta^{18}O_{spel}$ in Western Europe, as precipitation in some areas (mainly southern Europe) can originate from either the Atlantic or the Mediterranean, with the latter exhibiting higher $\delta^{18}O$ values [25,155,156] and wide range of total $\delta^{18}O$ variability. The differences in salinity and temperature between the two bodies of water determine the $\delta^{18}O$ of the moisture throughout the cloud trajectory, although other effects such as continentality, rainout effect or altitude also contribute to the final $\delta^{18}O$ signal. Moreover, changes in atmospheric circulation patterns can lead to shifts in moisture trajectories and seasonality of precipitation at a site (e.g., [157]). These effects have been recognised as partially influencing many of the records in SISAL_v1, mostly as second-order controls (e.g., Baschg [58], Ejulve [11,77], Grotta di Ernesto [44], Schafsloch [112], Schneckenloch [58,88], Seso [113]). The LGM portion of the composite record from Sieben Hengste (7H) Cave, is the only instance where $\delta^{18}O_{spel}$ was interpreted as principally reflecting changes between northerly and southerly moisture transport, informing on shifts in the meridional position of the North Atlantic storm track [114].

Due to these different factors potentially influencing $\delta^{18}O_{spel}$ in Western Europe, other climate proxies are often used to better constrain the palaeoclimatic interpretation of the records (e.g., $\delta^{13}C$ or trace element ratios) and their use should be promoted in the future. One possibility to quantitatively reconstruct the isotopic signature of the "parent" precipitation $\delta^{18}O$ is through fluid inclusion stable isotope analysis in speleothems [128,130]. Fluid inclusions provide a more direct record of precipitation $\delta^{18}O$ than speleothem calcite and allow the reconstruction of palaeo-temperatures when used in combination with carbonate $\delta^{18}O$, if this has precipitated at isotopic equilibrium [158]. To date, however, very few paleoclimate records

based on speleothem fluid inclusions exist (e.g., [129,130,159]) mostly because of the considerably larger effort required for their analysis and interpretation compared to carbonate $\delta^{18}O$. Much larger sample sizes are typically needed (~100 mg carbonate, compared to few tens of micrograms for carbonate $\delta^{18}O$), depending on the stalagmite growth rate and water content. Moreover, the analytical uncertainty is much higher than for carbonate (0.5‰ for $\delta^{18}O$ and 2‰ for δD, compared to 0.05–0.1‰ for carbonate $\delta^{18}O$; e.g., [160,161]). Thus, fluid inclusion isotope records remain less available for available for very high-resolution (up to subannual) studies that compose one of the main strengths of speleothems.

4. Regional Patterns in $\delta^{18}O_{spel}$ Records Through Time

4.1. Spatial Trends and Comparison to Observations

We use the SISAL database to detect whether present-day regional trends in $\delta^{18}O_{spel}$ values exist, and how they compare to trends in precipitation $\delta^{18}O$, taking advantage of the dense network of GNIP stations with long-term measurement records (up to 50 years). All analyses were referenced to the period 1958–2015. The average $\delta^{18}O_{spel}$ over this time period was calculated from the SISAL_v1 database ($n = 18$), while GNIP data was averaged over the entire year, after tests showed that averaging for winter months only gave the same result ($n = 211$; Figure 5). For a more direct comparison of SISAL_v1 $\delta^{18}O_{spel}$ and local precipitation data, we used the gridded interpolated precipitation data that is based on the GNIP network (background maps in Figure 5; [162,163]).
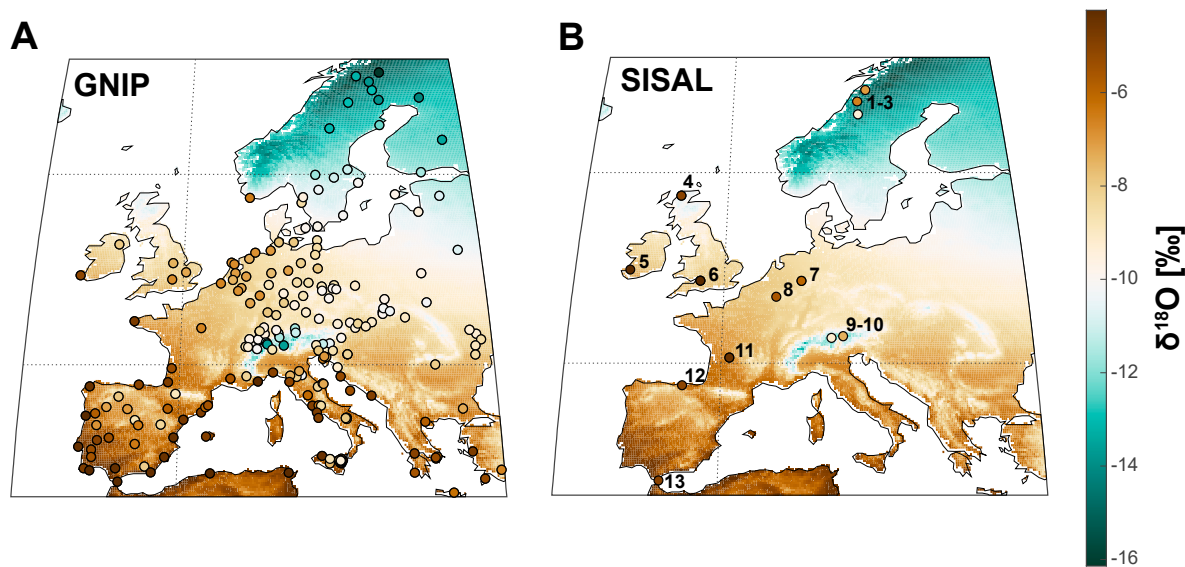
Figure 5. Comparison between: (**A**) GNIP station data, (**B**) average SISAL $\delta^{18}O$ values for the period 1958–2015 with interpolated GNIP data (background map: mean annual weighted $\delta^{18}O$ data from waterisotopes.org [163]). GNIP station data reflects calculated long-term annual means from stations with at least 10 months of data per year and five or more years of data ($n = 211$) and is shown as ‰ VSMOW. SISAL records (filled circles; $n = 18$) are averages over the period 1958–2013 and shown as ‰ VPDB. The SISAL records were not filtered to have a minimum number of data points, but only calcitic and aragonitic samples converted to calcite were included to avoid bias from mineralogy. Cave sites are numbered according to latitude: 1—Okshola [107], 2—Soylegrotta [45], 3—Korallgrottan [97], 4—Uamh an Tartair [123,124], 5—Crag [69,73], 6—Brown's Folly Mine [60,61], 7—Bunker [66], 8—Han-sur-Lesse [84], 9—Spannagel [116], 10—Klapferloch [95], 11—Villars [130], 12—Cueva de Asiul [74], 13—New St. Michael's [43,106].

Our comparison between SISAL sites and the GNIP interpolated precipitation data reveals moderate correlation (r^2 = 0.48, 18 sites, under the assumption of full independence between sites).

It is apparent from this comparison that high latitude SISAL sites are strongly offset from their corresponding precipitation $\delta^{18}O$ values (Figure 5B). The present-day spatial trends in $\delta^{18}O_{spel}$ reflect the dominant climatic processes reflected in precipitation $\delta^{18}O$ and provide the opportunity to establish "base lines" of $\delta^{18}O_{spel}$, to which high-frequency changes can be compared, as well as to check whether single isotope records might be anomalous within their regional climatic context [4]. On the whole, the spatial trend in $\delta^{18}O$ is very similar for precipitation and speleothems (Figure 5), and reflects increasing rainout away from the Atlantic (continental effect, [24]). Smaller-scale trends, such as the high $\delta^{18}O$ values found in the circum-Mediterranean region, and the altitude effect apparent in the Alpine region, are mirrored by the SISAL data.

Despite this good spatial agreement over Western Europe, discrepancies are apparent at some sites. Local conditions are known to affect speleothem geochemistry and need to be taken into account when developing transfer functions for climate reconstruction. The isotopically effective recharge [8], related to the dominant infiltration season and the degree of mixing in the karst aquifer, can substantially affect the correlation between $\delta^{18}O_{spel}$ and precipitation $\delta^{18}O$ [149,164]. Small-scale variability in mountain climate that is not captured by the interpolation approach used for the GNIP data is likely the reason for the offset between SISAL sites and the GNIP data in the Alpine region and northern Scandinavia (Figure 5; [32]).

4.2. Last Glacial Period

The SISAL_v1 database contains 24 records that cover the last glacial time period, i.e., the period between ~11.7 and ~115 ka (Figure 6). Many records from high altitude alpine cave sites show a very clear response to millennial-scale forcing from the North Atlantic (e.g., 7H, SPA 49, SPA 126, HOL-7, HOL-10, HOL-16-17, HOL-comp, BA-1, BA-1b, BA-2; Figure 6B). This strong synchronicity and similarity in the climatic response of the northern Alpine region and Greenland suggests a tight coupling between the two regions, which is likely related to the strong temperature control in these high altitude speleothems [87], and supported by data from other archives (e.g., [165]).

Speleothems from other cave sites in the region show a much less consistent pattern over the last glacial period, probably as a result of the complex interplay of processes affecting $\delta^{18}O_{spel}$ at mid-latitudes (Figure 6C). In some of these cases, the original authors used other geochemical proxies, such as $\delta^{13}C$, for the palaeoclimate interpretation. Stalagmites from Villars and Chauvet caves in France, for example, suggest a complex combination of temperature, precipitation amount and source changes affecting and muting their $\delta^{18}O_{spel}$, whereas $\delta^{13}C$ appears to be more sensitive to stadial-interstadial forcing. The authors interpret these rapid shifts in $\delta^{13}C$ as reflecting changes in soil CO_2 production, which is linked to temperature and humidity [67,126,127].
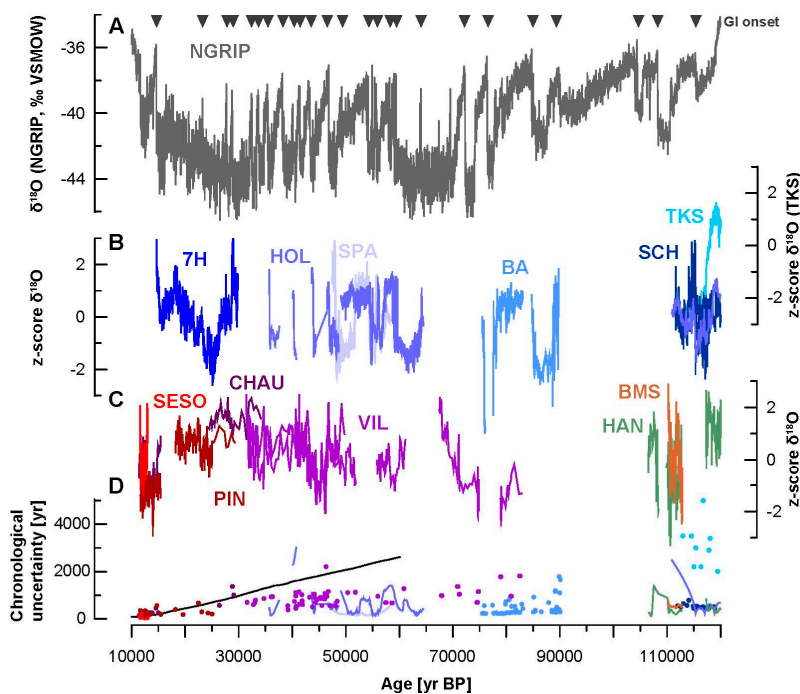
Figure 6. Examples of Western European records covering the last glacial period in SISAL_v1. To ease intercomparison of $\delta^{18}O_{spel}$, all records were normalised as z-scores. The onset of Greenland Interstadials (GIs) is indicated by the grey triangles [166,167]. (**A**) North Greenland Ice Core Project (NGRIP) ice core $\delta18O$ on the layer-counted GICC05modelext time scale for the last 60 kyrs, and extended further back on the ss09sea06bm time scale [167–169]. (**B**) Records from the Alpine region (colour coded): 7H—Composite record from Sieben Hengste Cave, Switzerland [114], SPA—Stalagmites SPA 49 and SPA 126, Kleegruben Cave, Austria [96], HOL—Stalagmites HOL-7 and HOL-10, composite records HOL-16-17 and HOL-comp from Hölloch Cave, Austria [87,88], BA—Stalagmites BA-1, BA-1b, and BA-2 from Baschg Cave, Austria [58], SCH—Stalagmites SCH-5 and SCH-7 from Schneckenloch Cave, Austria [58,88], TKS—Flowstone TKS from Entrische Kirche Cave, Austria [78]. Note that TKS is shown on a different y-axis to ease visual comparison. (**C**) Records from other parts of Western Europe (colour coded): SESO—Stalagmite SE09-6 from Seso Cave, Spain [113], PIN—Stalagmite Candela from El Pindal Cave, Spain [109,110], CHAU—Stalagmite Chau-stm6 from Chauvet Cave, France [67], VIL—Stalagmites Vil-stm9 and Vil-stm27 from Villars Cave, France [126,127], HAN—Stalagmite Han-9 from Han-sur-Lesse Cave, Belgium [85], BMS—Stalagmite BMS1 from Bue Marino Cave, Italy [65]. (**D**) Chronological uncertainty of the records: Speleothem U-Th ages are shown in colour coded dots. If available, the uncertainty of the age model is shown instead, as a more accurate measure of the time series uncertainty (lines). The black line indicates the maximum counting error of the layer-counted part of the ice core chronology [169].

4.3. Holocene Climate Variability

In our first assessment, we find no consistent regional trends in $\delta^{18}O_{spel}$ in SISAL_v1 records from Western Europe spanning the entire Holocene period. This is partly due to age modelling uncertainties and low temporal resolution in some records, which prevents the detection of climatic shifts in $\delta^{18}O_{spel}$ during periods with low signal-to-noise ratios. Although Holocene climate conditions are more stable than during the last glacial period, recent evidence suggests significant variability, challenging the notion of a "very stable Holocene" [170]. The 8.2 ka event, a significant North Atlantic focused temperature event, can be used as a benchmark to test the sensitivity of our records for millennial-scale climate change. In SISAL_v1, 21 records from Western Europe cover the time period around 8.2 ka, and nine of them were

interpreted by the original authors as recording evidence for a climatic perturbation at that time (Figure 7). Another four show changes in their growth and petrography (i.e., hiatuses, erosional surfaces, changes in calcite fabrics) that can tentatively be related to climate change around 8.2 ka. For most of the records, however, chronological uncertainty and/or temporal resolution remain an issue, and the detailed structure and timing of the 8.2 ka event often cannot be resolved (Figure 7). As a result of the paucity of available datasets it is also not possible at this stage to assess any regional trends in the expression of the 8.2 ka event in stalagmites from Western Europe. Recent advances in analytical and sampling methods provide an opportunity for future studies to obtain more detailed insights into this event, both in previously sampled records and at new sites. Such investigations might also help in disentangling the 8.2 ka event in Western Europe from underlying low-frequency climatic events at that time [171].
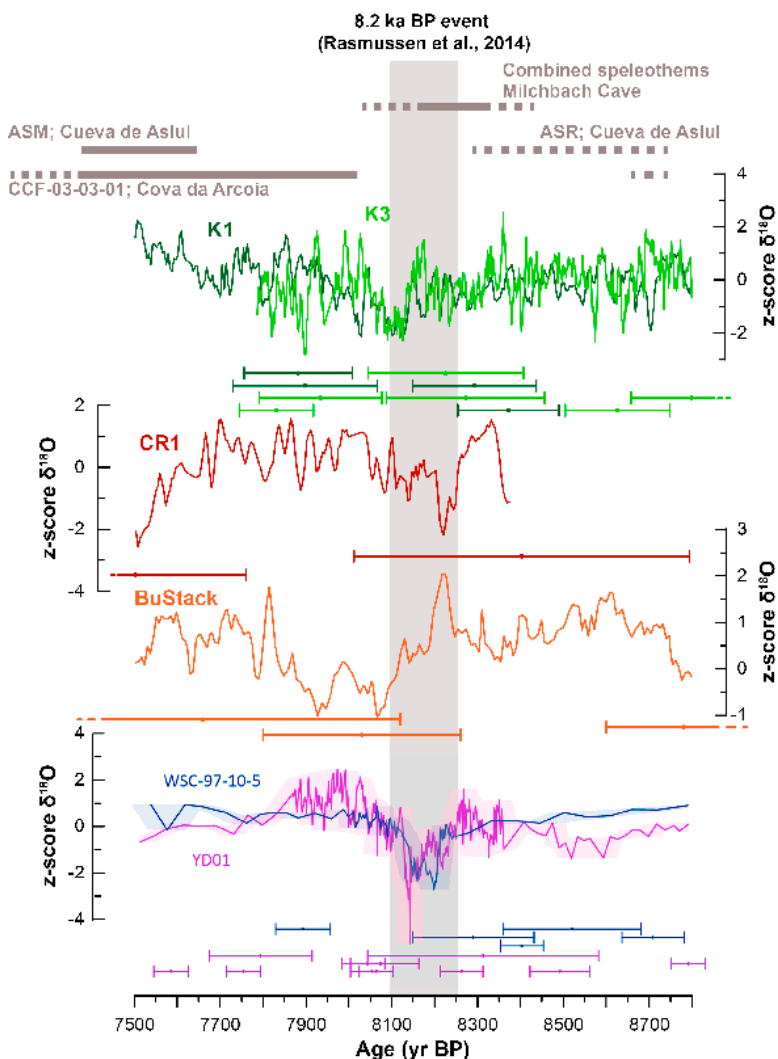
Figure 7. Examples of Western European records in SISAL showing evidence for a climatic perturbation over the 8.2 ka event. To facilitate intercomparison of $\delta^{18}O_{spel}$, all records were normalised as z-scores. The duration of the 8.2 ka event is shown with the grey bar [166]. K1, K3—Stalagmites from Katerloch Cave, Austria [93], CR1—Stalagmite from Grotta di Carburangeli, Italy [80], BuStack—Composite record from Bunker Cave, Germany [66], WSC-97-10-5—Stalagmite from White Scar Cave, England [111], YD01—

Stalagmite from Pippikin Pot Cave, England [111]. Ages with respective 2σ uncertainties are shown below each record. For WSC-97-10-5 and YD01, the uncertainties of the age model are also shown (shaded error bars underlying the time series). Note that the uncertainty of the Bunker Cave composite record is likely smaller than suggested by the single U-Th ages, due to overlap of single stalagmite records, but this information was not available in SISAL_v1 [66]. Stalagmites with petrographic or growth rate evidence for a climatic event are shown in grey bars at the top: A glacier advance is suggested by petrographic changes in stalagmites from Milchbach Cave, Switzerland [104], growth cessation/start around the event is recorded by stalagmites ASR and ASM from Cueva de Asiul, Spain [74], and an erosional surface is found in stalagmite ESP03 from Cova da Arcoia, Spain [71].

4.4. The Last Two Millennia

We evaluated the regional coherency of $\delta^{18}O_{spel}$ over the last two millennia using the data in SISAL_v1 by stacking all records covering at least 1/3 of the interval (−50–2000 yr BP) at reasonable resolution (≥10 data points), and for which an age model is available. Eighteen records fulfil these requirements: Stalagmites Vil-stm1 and Vil-stm6 from Villars Cave, France [130]; stalagmites LH-70s-2 and LH-70s-3 from Lancaster Hole, England [102]; stalagmite SU967 from Uamh an Tartair Cave, Scotland [123]; stalagmite FM3 from Okshola Cave, Norway [107]; stalagmite L03 from Larshullet Cave, Norway [103]; stalagmite SG05 from Soylegrotta Cave, Norway [45]; stalagmite K11 from Korallgrottan Cave, Sweden [97]; the composite record from the Austrian Alps COMNISPAII [116], stalagmite CC3 from Crag Cave, Ireland [69]; flowstone PFU6 from Klapferloch Cave, Austria [95]; stalagmite CL26 from Clamouse Cave, France [69]; the composite record from Bunker Cave, Germany [66]; stalagmites ASR and ASM from Cueva de Asiul, Spain [74]; flowstone RL4 from Buca della Renella, Italy [63]; and stalagmite ESP03 from Cova da Arcoia, Spain [71]. After a Gaussian smoothing on a 100-year timescale was performed for all records, they were interpolated to 5-year timescales. For the stack, the unweighted average of all records was used, and no weighting based on location, correlation strength, or uncertainty was performed.

The stacked record for the last 2000 years shows a long-term trend towards more positive $\delta^{18}O_{spel}$ between 2000–550 yr BP, followed by a reversal (Figure 8). The highest $\delta^{18}O_{spel}$ values of the stack at 550 yr BP fall within the Little Ice Age (LIA; [175]). However there is no clear indication of systematic changes in $\delta^{18}O_{spel}$ corresponding to the Roman Warm Period (RWP; [177]), the Late Antique Little Ice Age (LALIA; [177]), or the Medieval Climate Anomaly (MCA; [176]), periods of significant temperature change in Europe. This failure may reflect the high uncertainties related to the degree of noise in the single speleothem records, as well as the different climate signals recorded by the individual speleothems. It is important to note that the stack captures the mean $\delta^{18}O_{spel}$ signal in Western Europe, and not a single climate process, e.g., temperature or precipitation amount. A screening of the records based on their response to climate was not possible at present, since most records are not calibrated against instrumental data. If more records that fulfil this requirement become available, a stack based on the recorded climate process might become feasible. In addition, future improvements of this procedure should tackle a regional assessment of the trends using a higher number of records and possibly including proxy data from other archives, checking correlations between nearby records, incorporating age uncertainties, and the integration of the signal's interpretation by the original authors.
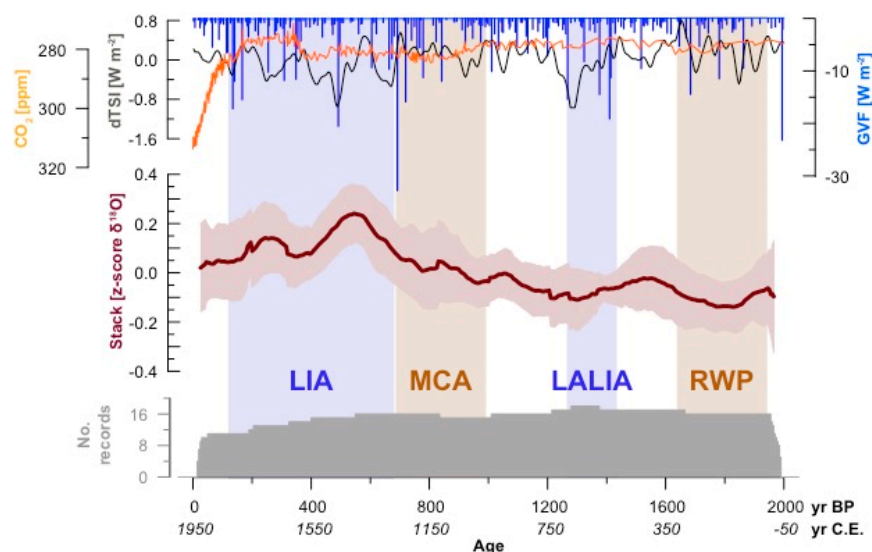
Figure 8. Stacked record of SISAL entities covering the last 2000 years, compared to global climate forcings: Global Volcanic Forcing (GVF; [172]), solar forcing (total solar insolation anomalies, dTSI; [173]), and CO_2 concentrations from combined ice core records [174]. Important climate periods are indicated, and defined according to the following references: Little Ice Age (LIA; [175]), Medieval Climate Anomaly (MCA; [176]), Late Antique Little Ice Age (LALIA), and Roman Warm Period (RWP; [177]).

5. Improvements to SISAL for Western Europe

Only 60% of the known records from Western Europe are in the SISAL_v1 database and the remaining records not yet in SISAL are widely distributed across Europe (Austria: 22, Belgium: 3, France: 7, Germany: 5, Italy: 3, Norway: 5, Spain: 9, Sweden: 1, Switzerland: 2). We have shown, for the current version of the database, that the speleothem records from Western Europe have potential to document some aspects of past climate change. However, it is clear that outstanding issues need to be addressed first, which in Western Europe can be summarised as (i) improvement of temporal coverage, (ii) improvement of spatial coverage, especially with records calibrated against modern climate conditions, and (iii) a more comprehensive use of statistical approaches to extract underlying modes from spatially distributed records, a key aim of the SISAL working group.

Overall, the paucity of records spanning beyond the LGM presents an opportunity for future studies to target speleothems covering previous time periods, especially given their often more precise U-Th chronologies at these time scales compared to ice cores and marine sediment records [11,178,179]. Climate variability over the last glacial and beyond remains poorly constrained and speleothems could provide detailed information from vast range of different environments (coastal, continental, high altitude/latitude, etc.).

Modern records that contribute to improving our assessment of the spatial robustness of $\delta^{18}O_{spel}$ in Western Europe need to be calibrated against modern conditions, taking advantage of the GNIP network and climate model simulations. This is particularly important for the goals outlined by SISAL, as $\delta^{18}O$ is by far the most reported speleothem geochemical proxy, and the only one that has a direct parameter equivalent in climate model simulations with isotopic tracers. Instrumental and modelling data have recently allowed to define regions within Western Europe that are particularly suited for reconstructions of certain (hydro-)climatic conditions, especially with respect to spatio-temporal non-stationarities of the NAO [29,31,32]. In particular, variable sensitivities to the NAO have been implied for Central Europe, the Iberian Peninsula, the Baltic Sea, the British Isles, and the circum-Mediterranean region [32].

Record coverage in these areas is still patchy (Figure 1), and should be targeted by future efforts, ideally including long-term cave microclimate monitoring to define present day surface to cave transport processes, assessment of local hydroclimate variability (through the isotopic analysis of precipitation samples from the cave site), and careful sampling practices.

Competing influences on $\delta^{18}O_{spel}$ and low signal-to-noise ratios at mid-latitude sites still prevent a quantitative interpretation of $\delta^{18}O$. As recently demonstrated by Deininger et al. [33], who used Monte Carlo based Principal Component Analysis on several $\delta^{18}O_{spel}$ records in the same region, sophisticated statistics methods can extract a common mode of climate variability from these datasets. Our approach of stacking different records is also useful to determine robust regional trends in a quantitative manner, but needs to be refined by future studies. Such statistical approaches hold great promise in the context of a large database like SISAL and could be used to better constrain spatial trends in precipitation $\delta^{18}O$ over time, and improve our understanding of local and regional influences on $\delta^{18}O_{spel}$.

6. Future Directions

This first assessment of the Western European data compiled in the SISAL_v1 database highlights interesting spatial and temporal trends in stalagmite $\delta^{18}O$, but these will need to be validated and better constrained by future work on the database. Specifically, we encourage:

- Inclusion of missing records, which were not available to us for SISAL_v1 as they had not been archived in the supplementary information or on public repositories, and where no/limited contact with the original authors could be established. This is crucial for the assessment of temporal and spatial coverage of speleothem records in Western Europe and helps defining future target regions and time periods for new studies. This could be a starting point for revisiting sites and speleothems that have shown great sensitivity for climate reconstruction, but where resolution and/or chronological precision could be improved. It could also be of interest for a better definition of short-lived events such as the 8.2 ka event or the 4.2 ka event, and to improve chronological controls of speleothems previously dated with TIMS.
- Addition and use of other types of data. For example, fluid inclusion $\delta^{18}O$ measurements on speleothems would provide important direct information on past precipitation $\delta^{18}O$. Similarly, speleothem $\delta^{13}C$ data, already included in the database, should be evaluated, as many sites highlight its importance as (qualitative) proxy for soil activity and hydroclimate [44,61,126].
- Inclusion of more information about cave monitoring. The SISAL_v1 database only includes a yes/no/unknown entry for cave monitoring, which is often not sufficient when evaluating the extent of knowledge of modern cave conditions.

7. Conclusions

By assessing the speleothem data collected in the SISAL_v1 database for Western Europe, we describe regional trends in $\delta^{18}O$, and evaluate the potential of this large compilation of records for palaeoclimate studies in this region. Western Europe has the largest number of published speleothem palaeoclimate records worldwide, many of which (>60% of the identified records) are currently included in SISAL_v1. Moreover, climate conditions are well understood, due to the availability of a dense network of GNIP stations, some of the longest meteorological records worldwide, and global modelling and reanalysis datasets. This is a great advantage for the interpretation of $\delta^{18}O_{spel}$ records, which at mid-latitude sites is often difficult because of competing effects from precipitation and cave processes.

In this review of Western European data included in SISAL_v1, we find that (i) present-day spatial trends in $\delta^{18}O_{spel}$ from Western European caves generally mirror the trends in precipitation $\delta^{18}O$. (ii) Over the late Quaternary, site-specific noise in $\delta^{18}O_{spel}$ presents the main issue for the extraction of a regional

climate signal, especially over the Holocene. (iii) Encouraging results can be obtained through the use of statistical methods, which allow the extraction of regional climate modes.

　　The SISAL database is a valuable tool for the intercomparison of $\delta^{18}O_{spel}$ records over the Western European region. We believe this will provide an important resource of palaeoclimatic input for modelling studies and improve our understanding of the speleothem archive at mid-latitude regions.

References

1.　Wong, C.I.; Breecker, D.O. Advancements in the use of speleothems as climate archives. *Quat. Sci. Rev.* **2015**, *127*, 1–18. [CrossRef]

2.　Henderson, G.M. Caving in to new chronologies. *Science* **2006**, *313*, 620–622. [CrossRef] [PubMed]

3.　Atsawawaranunt, K.; Comas-Bru, L.; Mozhdehi, S.A.; Deininger, M.; Harrison, S.P.; Baker, A.; Boyd, M.; Kaushal, N.; Ahmad, S.M.; Ait Brahim, Y.; et al. The SISAL database: A global resource to document oxygen and carbon isotope records from speleothems. *Earth Syst. Sci. Data* **2018**, *10*, 1687–1713. [CrossRef]

4.　McDermott, F.; Atkinson, T.C.; Fairchild, I.J.; Baldini, L.M.; Mattey, D.P. A first evaluation of the spatial gradients in δ18O recorded by European Holocene speleothems. *Glob. Planet. Chang.* **2011**, *79*, 275–287. [CrossRef]

5.　Duplessy, J.C.; Labeyrie, J.; Lalou, C.; Nguyen, H.V. Continental climatic variations between 130,000 and 90,000 years BP. *Nature* **1970**, *226*, 631–633. [CrossRef] [PubMed]

6.　Lauritzen, S.-E.; Lundberg, J. Speleothems and climate: A special issue of The Holocene. *Holocene* **1999**, *9*, 643–647. [CrossRef]

7.　McDermott, F. Palaeo-climate reconstruction from stable isotope variations in speleothems: A review. *Quat. Sci. Rev.* **2004**, *23*, 901–918. [CrossRef]

8.　Lachniet, M.S. Climatic and environmental controls on speleothem oxygen-isotope values. *Quat. Sci. Rev.* **2009**, *28*, 412–432. [CrossRef]

9.　Wanner, H.; Beer, J.; Bütikofer, J.; Crowley, T.J.; Cubasch, U.; Flückiger, J.; Goosse, H.; Grosjean, M.; Joos, F.; Kaplan, J.O.; et al. Mid- to Late Holocene climate change: An overview. *Quat. Sci. Rev.* **2008**, *27*, 1791–1828. [CrossRef]

10.　Wassenburg, J.A.; Dietrich, S.; Fietzke, J.; Fohlmeister, J.; Jochum, K.P.; Scholz, D.; Richter, D.K.; Sabaoui, A.; Spötl, C.; Lohmann, G.; et al. Reorganization of the North Atlantic Oscillation during early Holocene deglaciation. *Nat. Geosci.* **2016**, *9*, 602–605. [CrossRef]

11. Pérez-Mejías, C.; Moreno, A.; Sancho, C.; Bartolomé, M.; Stoll, H.; Cacho, I.; Cheng, H.; Edwards, R.L. Abrupt climate changes during Termination III in Southern Europe. *Proc. Natl. Acad. Sci. USA* **2017**, *114*, 10047–10052. [CrossRef] [PubMed]

12. IAEA/WMO. Global Network of Isotopes in Precipitation. The GNIP Database. 2018. Available online: https://nucleus.iaea.org/wiser (accessed on 10 October 2018).

13. Genty, D. Palaeoclimate Research in Villars Cave (Dordogne, SW-France). *Int. J. Speleol.* **2008**, *37*, 173–191. [CrossRef]

14. Spötl, C.; Fairchild, I.J.; Tooth, A.F. Cave air control on dripwater geochemistry, Obir Caves (Austria): Implications for speleothem deposition in dynamically ventilated caves. *Geochim. Cosmochim. Acta* **2005**, *69*, 2451–2468. [CrossRef]

15. Sundqvist, H.S.; Seibert, J.; Holmgren, K. Understanding conditions behind speleothem formation in Korallgrottan, northwestern Sweden. *J. Hydrol.* **2007**, *347*, 13–22. [CrossRef]

16. Genty, D.; Labuhn, I.; Hoffmann, G.; Danis, P.A.; Mestre, O.; Bourges, F.; Wainer, K.; Massault, M.; Van Exter, S.; Régnier, E.; et al. Rainfall and cave water isotopic relationships in two South-France sites. *Geochim. Cosmochim. Acta* **2014**, *131*, 323–343. [CrossRef]

17. Riechelmann, S.; Schröder-Ritzrau, A.; Spötl, C.; Riechelmann, D.F.C.; Richter, D.K.; Mangini, A.; Frank, N.; Breitenbach, S.F.M.; Immenhauser, A. Sensitivity of Bunker Cave to climatic forcings highlighted through multi-annual monitoring of rain-, soil-, and dripwaters. *Chem. Geol.* **2017**, *449*, 194–205. [CrossRef]

18. Kern, Z.; Demény, A.; Hatvani, I.G. Speleothem records from Eastern Europe & Turkey. *Quaternary* **2018**, submitted.

19. Chen, Z.; Auler, A.S.; Bakalowicz, M.; Drew, D.; Griger, F.; Hartmann, J.; Jiang, G.; Moosdorf, N.; Richts, A.; Stevanovic, Z.; et al. The World Karst Aquifer Mapping project: Concept, mapping procedure and map of Europe. *Hydrogeol. J.* **2017**, *25*, 771–785. [CrossRef]

20. Comas-Bru, L.; Harrison, S.P.; Deininger, M. SISAL, speleothems and the state-of-the-art. *Quaternary* **2018**, submitted.

21. Kottek, M.; Grieser, J.; Beck, C.; Rudolf, B.; Rubel, F. World map of the Köppen-Geiger climate classification updated. *Meteorol. Z.* **2006**, *15*, 259–263. [CrossRef]

22. Geiger, R. Überarbeitete Neuausgabe von Geiger, R. In *Köppen-Geiger/Klima der Erde. (Wandkarte 1:16 Mill)*; Klett-Perthes: Gotha, Germany, 1961.

23. Geiger, R. Klassifikation der klimate nach W. Köppen. In *Landolt-Börnstein, Zahlenwerte und Funktionen aus Physik, Chemie, Astronomie, Geophysik und Technik*; Alte Series; Springer: Berlin, Germany, 1954; Volume 3.

24. Rozanski, K.; Araguás-Araguás, L.; Gonfiantini, R. Isotopic patterns in modern global precipitation. In *Climate Change in Continental Isotopic Records*; Swart, P.K., Lohmann, K.C., McKenzie, J., Savin, S., Eds.; AGU: Washington, DC, USA, 1993; pp. 1–36.

25. Celle-Jeanton, H.; Travi, Y.; Blavoux, B. Isotopic typology of the precipitation in the Western Mediterrenean region at the three different time scales. *Geophys. Res. Lett.* **2001**, *28*, 1215–1218. [CrossRef]

26. Flaim, G.; Camin, F.; Tonon, A.; Obertegger, U. Stable isotopes of lakes and precipitation along an altitudinal gradient in the Eastern Alps. *Biogeochemistry* **2013**, *116*, 187–198. [CrossRef]

27. Hurrell, J.W.; Deser, C. North Atlantic climate variability: The role of the North Atlantic Oscillation. *J. Mar. Syst.* **2009**, *78*, 28–41. [CrossRef]

28. Marshall, J.; Kushnir, Y.; Battisti, D.; Chang, P.; Czaja, A.; Dickson, R.; Hurrell, J.; McCartney, M.; Saravanan, R.; Visbeck, M. North Atlantic climate variability: Phenomena, impacts and mechanisms. *Int. J. Climatol.* **2001**, *21*, 1863–1898. [CrossRef]

29. Casty, C.; Wanner, H.; Luterbacher, J.; Esper, J.; Böhm, R. Temperature and precipitation variability in the European Alps since 1500. *Int. J. Climatol.* **2005**, *25*, 1855–1880. [CrossRef]

30. Fischer, M.J.; Mattey, D. Climate variability and precipitation isotope relationships in the Mediterranean region. *J. Geophys. Res. Atmos.* **2012**, *117*, 1–13. [CrossRef]

31. Baldini, L.M.; McDermott, F.; Foley, A.M.; Baldini, J.U.L. Spatial variability in the European winter precipitation d18O-NAO relationship: Implications for reconstructing NAO-mode climate variability in the Holocene. *Geophys. Res. Lett.* **2008**. [CrossRef]
32. Comas-Bru, L.; McDermott, F.; Werner, M. The effect of the East Atlantic pattern on the precipitation δ18O-NAO relationship in Europe. *Clim. Dyn.* **2016**, *47*, 2059–2069. [CrossRef]
33. Deininger, M.; McDermott, F.; Mudelsee, M.; Werner, M.; Frank, N.; Mangini, A. Coherency of late Holocene European speleothem δ18O records linked to North Atlantic Ocean circulation. *Clim. Dyn.* **2017**, *49*, 595–618. [CrossRef]
34. Langebroek, P.M.; Werner, M.; Lohmann, G. Climate information imprinted in oxygen-isotopic composition of precipitation in Europe. *Earth Planet. Sci. Lett.* **2011**, *311*, 144–154. [CrossRef]
35. Field, R.D. Observed and modeled controls on precipitation δ18O over Europe: From local temperature to the Northern Annular Mode. *J. Geophys. Res. Atmos.* **2010**, *115*. [CrossRef]
36. Moore, G.W.K.; Pickart, R.S.; Renfrew, I.A. Complexities in the climate of the subpolar North Atlantic: A case study from the winter of 2007. *Q. J. R. Meteorol. Soc.* **2011**, *137*, 757–767. [CrossRef]
37. Moore, G.W.K.; Renfrew, I.A.; Pickart, R.S. Multidecadal mobility of the North Atlantic Oscillation. *J. Clim.* **2013**, *26*, 2453–2466. [CrossRef]
38. Comas-Bru, L.; McDermott, F. Impacts of the EA and SCA patterns on the European twentieth century NAO-winter climate relationship. *Q. J. R. Meteorol. Soc.* **2014**, *140*, 354–363. [CrossRef]
39. Martin-Vide, J.; Lopez-Bustins, J.-A. The Western Mediterranean Oscillation and rainfall in the Iberian Peninsula. *Int. J. Climatol.* **2006**, *26*, 1455–1475. [CrossRef]
40. Harris, I.; Jones, P.D.; Osborn, T.J.; Lister, D.H. Updated high-resolution grids of monthly climatic observations—The CRU TS3.10 Dataset. *Int. J. Climatol.* **2014**, *34*, 623–642. [CrossRef]
41. Drysdale, R.N.; Zanchetta, G.; Hellstrom, J.C.; Fallick, A.E.; Zhao, J.X.; Isola, I.; Bruschi, G. Palaeoclimatic implications of the growth history and stable isotope (d18O and d13C) geochemistry of a Middle to Late Pleistocene stalagmite from central-western Italy. *Earth Planet. Sci. Lett.* **2004**, *227*, 215–229. [CrossRef]
42. Drysdale, R.N.; Zanchetta, G.; Hellstrom, J.C.; Fallick, A.E.; Zhao, J.X. Stalagmite evidence for the onset of the Last Interglacial in southern Europe at 129 +/−1 ka. *Geophys. Res. Lett.* **2005**, *32*, 1–4. [CrossRef]
43. Mattey, D.; Lowry, D.; Duffet, J.; Fisher, R.; Hodge, E.; Frisia, S. A 53 year seasonally resolved oxygen and carbon isotope record from a modern Gibraltar speleothem: Reconstructed drip water and relationship to local precipitation. *Earth Planet. Sci. Lett.* **2008**, *269*, 80–95. [CrossRef]
44. Scholz, D.; Frisia, S.; Borsato, A.; Spötl, C.; Fohlmeister, J.; Mudelsee, M.; Miorandi, R.; Mangini, A. Holocene climate variability in north-eastern Italy: Potential influence of the NAO and solar activity recorded by speleothem data. *Clim. Past* **2012**, *8*, 1367–1383. [CrossRef]
45. Linge, H.; Lauritzen, S.-E.; Lundberg, J. Stable isotope stratigraphy of a late Last Interglacial speleothem from Rana, Northern Norway. *Quat. Res.* **2001**, *56*, 155–164. [CrossRef]
46. Berstad, I.M.; Lundberg, J.; Lauritzen, S.E.; Linge, H. Comparison of the climate during marine isotope stage 9 and 11 inferred from a speleothem isotope record from northern Norway. *Quat. Res.* **2002**, *58*, 361–371. [CrossRef]
47. Lauritzen, S.-E.; Lundberg, J. Isotope Stage 11, the "Super-Interglacial", from a north Norwegian speleothem. In *Studies of Cave Sediments*; Springer: Boston, MA, USA, 2004; pp. 257–272.
48. Scroxton, N.; Gagan, M.K.; Dunbar, G.B.; Ayliffe, L.K.; Hantoro, W.S.; Shen, C.C.; Hellstrom, J.C.; Zhao, J.X.; Cheng, H.; Edwards, R.L.; et al. Natural attrition and growth frequency variations of stalagmites in southwest Sulawesi over the past 530,000 years. *Palaeogeogr. Palaeoclimatol. Palaeoecol.* **2016**, *441*, 823–833. [CrossRef]
49. Fischer, H.; Meissner, K.J.; Mix, A.C.; Abram, N.J.; Austermann, J.; Brovkin, V.; Capron, E.; Colombaroli, D.; Daniau, A.L.; Dyez, K.A.; et al. Palaeoclimate constraints on the impact of 2°C anthropogenic warming and beyond. *Nat. Geosci.* **2018**, *11*, 474–485. [CrossRef]
50. Lisiecki, L.E.; Raymo, M.E. A Pliocene-Pleistocene stack of 57 globally distributed benthic d18O records. *Paleoceanography* **2005**, *20*, 1–17. [CrossRef]

51. Drysdale, R.N.; Zanchetta, G.; Hellstrom, J.C.; Fallick, A.E.; McDonald, J.; Cartwright, I. Stalagmite evidence for the precise timing of North Atlantic cold events during the early last glacial. *Geology* **2007**, *35*, 77–80. [CrossRef]

52. Drysdale, R.N.; Hellstrom, J.C.; Zanchetta, G.; Fallick, A.E.; Sanchez Goni, M.F.; Couchoud, I.; McDonald, J.; Maas, R.; Lohmann, G.; Isola, I. Evidence for obliquity forcing of Glacial Termination II. *Science* **2009**, *325*, 1527–1531. [CrossRef]

53. Daëron, M.; Guo, W.; Eiler, J.; Genty, D.; Blamart, D.; Boch, R.; Drysdale, R.; Maire, R.; Wainer, K.; Zanchetta, G. $^{13}C^{18}O$ clumping in speleothems: Observations from natural caves and precipitation experiments. *Geochim. Cosmochim. Acta* **2011**, *75*, 3303–3317.

54. Zanchetta, G.; Drysdale, R.N.; Hellstrom, J.C.; Fallick, A.E.; Isola, I.; Gagan, M.K.; Pareschi, M.T. Enhanced rainfall in the Western Mediterranean during deposition of sapropel S1: stalagmite evidence from Corchia cave (Central Italy). *Quat. Sci. Rev.* **2007**, *26*, 279–286. [CrossRef]

55. Jackson, A.S.; McDermott, F.; Mangini, A. Late Holocene climate oscillations and solar fluctuations from speleothem STAL-AH-1, Sauerland, Germany: A numerical perspective. *Geophys. Res. Lett.* **2008**, *35*, 1–5. [CrossRef]

56. Niggemann, S.; Mangini, A.; Mudelsee, M.; Richter, D.K.; Wurth, G. Sub-Milankovitch climatic cycles in Holocene stalagmites from Sauerland, Germany. *Earth Planet. Sci. Lett.* **2003**, *216*, 539–547. [CrossRef]

57. Niggemann, S.; Mangini, A.; Richter, D.K.; Wurth, G. A paleoclimate record of the last 17,600 years in stalagmites from the B7 cave, Sauerland, Germany. *Quat. Sci. Rev.* **2013**, *22*, 555–567. [CrossRef]

58. Boch, R.; Cheng, H.; Spötl, C.; Edwards, R.L.; Wang, X.; Häuselmann, P. NALPS: A precisely dated European climate record 120-60 ka. *Clim. Past* **2011**, *7*, 1247–1259. [CrossRef]

59. Couchoud, I.; Genty, D.; Hoffmann, D.; Drysdale, R.; Blamart, D. Millennial-scale climate variability during the Last Interglacial recorded in a speleothem from south-western France. *Quat. Sci. Rev.* **2009**, *28*, 3263–3274. [CrossRef]

60. Baldini, J.U.L. Morphologic and dimensional linkage between recently deposited speleothems and drip water from Browns Folly Mine, Wiltshire, England. *J. Cave Karst Stud.* **2001**, *63*, 83–90.

61. Baldini, J.U.L.; McDermott, F.; Baker, A.; Baldini, L.M.; Mattey, D.P.; Railsback, L.B. Biomass effects on stalagmite growth and isotope ratios: A 20th century analogue from Wiltshire, England. *Earth Planet. Sci. Lett.* **2005**, *240*, 486–494. [CrossRef]

62. Drysdale, R.; Zanchetta, G.; Hellstrom, J.; Maas, R.; Fallick, A.; Pickett, M.; Cartwright, I.; Piccini, L. Late Holocene drought responsible for the collapse of Old World civilizations is recorded in an Italian cave flowstone. *Geology* **2006**, *34*, 101–104. [CrossRef]

63. Zanchetta, G.; Regattieri, E.; Isola, I.; Drysdale, R.N.; Bini, M.; Baneschi, I.; Hellstrom, J.C. The so-called "4.2 event" in the central mediterranean and its climatic teleconnections. *Alp. Mediterr. Quat.* **2016**, *29*, 5–17.

64. Drysdale, R.N. Unpublished dataset. 2018.

65. Columbu, A.; Drysdale, R.; Capron, E.; Woodhead, J.; De Waele, J.; Sanna, L.; Hellstrom, J.; Bajo, P. Early last glacial intra-interstadial climate variability recorded in a Sardinian speleothem. *Quat. Sci. Rev.* **2017**, *169*, 391–397. [CrossRef]

66. Fohlmeister, J.; Schröder-Ritzrau, A.; Scholz, D.; Spötl, C.; Riechelmann, D.F.C.; Mudelsee, M.; Wackerbarth, A.; Gerdes, A.; Riechelmann, S.; Immenhauser, A.; et al. Bunker cave stalagmites: An archive for central European Holocene climate variability. *Clim. Past* **2012**, *8*, 1751–1764. [CrossRef]

67. Genty, D.; Blamart, D.; Ghaleb, B.; Plagnes, V.; Causse, C.; Bakalowicz, M.; Zouari, K.; Chkir, N.; Hellstrom, J.; Wainer, K.; et al. Timing and dynamics of the last deglaciation from European and North African δ13C stalagmite profiles-comparison with Chinese and South Hemisphere stalagmites. *Quat. Sci. Rev.* **2006**, *25*, 2118–2142. [CrossRef]

68. Plagnes, V.; Causse, C.; Genty, D.; Paterne, M.; Blamart, D. A discontinuous climatic record from 187 to 74 ka from a speleothem of the Clamouse Cave (south of France). *Earth Planet. Sci. Lett.* **2002**, *201*, 87–103. [CrossRef]

69. McDermott, F.; Frisia, S.; Huang, Y.; Longinelli, A.; Spiro, B.; Heaton, T.H.E.; Hawkesworth, C.J.; Borsato, A.; Keppens, E.; Fairchild, I.J.; et al. Holocene climate variability in Europe: Evidence from d18O, textural and extension-rate variations in three speleothems. *Quat. Sci. Rev.* **1999**, *18*, 1021–1038. [CrossRef]

70. Genty, D.; Plagnes, V.; Causse, C.; Cattani, O.; Stievenard, M.; Falourd, S.; Blamart, D.; Ouahdi, R.; Van-Exter, S. Fossil water in large stalagmite voids as a tool for paleoprecipitation stable isotope composition reconstitution and paleotemperature calculation. *Chem. Geol.* **2002**, *184*, 83–95. [CrossRef]

71. Railsback, L.B.; Liang, F.; Vidal Romaní, J.R.; Grandal-d'Anglade, A.; Vaqueiro Rodríguez, M.; Santos Fidalgo, L.; Fernández Mosquera, D.; Cheng, H.; Edwards, R.L. Petrographic and isotopic evidence for Holocene long-term climate change and shorter-term environmental shifts from a stalagmite from the Serra do Courel of northwestern Spain, and implications for climatic history across Europe and the Mediterranean. *Palaeogeogr. Palaeoclimatol. Palaeoecol.* **2011**, *305*, 172–184. [CrossRef]

72. Hodge, E.J.; Richards, D.A.; Smart, P.L.; Andreo, B.; Hoffmann, D.L.; Mattey, D.P.; González-Ramón, A. Effective precipitation in southern Spain (∼266 to 46 ka) based on a speleothem stable carbon isotope record. *Quat. Res.* **2008**, *69*, 447–457. [CrossRef]

73. McDermott, F.; Mattey, D.P.; Hawkesworth, C. Centennial-scale holocene climate variability revealed by a high-resolution speleothemd18O record from SW Ireland. *Science* **2001**, *294*, 1328–1331. [CrossRef]

74. Smith, A.C.; Wynn, P.M.; Barker, P.A.; Leng, M.J.; Noble, S.R.; Tych, W. North Atlantic forcing of moisture delivery to Europe throughout the Holocene. *Sci. Rep.* **2016**, *6*. [CrossRef]

75. Martín-Chivelet, J.; Muñoz-García, M.B.; Edwards, R.L.; Turrero, M.J.; Ortega, A.I. Land surface temperature changes in Northern Iberia since 4000yrBP, based on $\delta 13C$ of speleothems. *Glob. Planet. Chang.* **2011**, *77*, 1–12.

76. González-Lemos, S.; Jiménez-Sánchez, M.; Stoll, H.M. Sediment transport during recent cave flooding events and characterization of speleothem archives of past flooding. *Geomorphology* **2015**, *228*, 87–100.

77. Moreno, A.; Pérez-Mejías, C.; Bartolomé, M.; Sancho, C.; Cacho, I.; Stoll, H.; Delgado-Huertas, A.; Hellstrom, J.; Edwards, R.L.; Cheng, H. New speleothem data from Molinos and Ejulve caves reveal Holocene hydrological variability in northeast Iberia. *Quat. Res.* **2017**, *88*, 223–233. [CrossRef]

78. Meyer, M.C.; Spötl, C.; Mangini, A. The demise of the Last Interglacial recorded in isotopically dated speleothems from the Alps. *Quat. Sci. Rev.* **2008**, *27*, 476–496. [CrossRef]

79. Ponte, J.M.; Font, E.; Veiga-Pires, C.; Hillaire-Marcel, C.; Ghaleb, B. The effect of speleothem surface slope on the remanent magnetic inclination. *J. Geophys. Res. Solid Earth* **2017**, *122*, 4143–4156. [CrossRef]

80. Frisia, S.; Borsato, A.; Mangini, A.; Spötl, C.; Madonia, G.; Sauro, U. Holocene climate variability in Sicily from a discontinuous stalagmite record and the Mesolithic to Neolithic transition. *Quat. Res.* **2006**, *66*, 388–400. [CrossRef]

81. Madonia, G.; Frisia, S.; Borsato, A.; Macaluso, T.; Mangini, A.; Paladini, M.; Piccini, L.; Miorandi, R.; Spötl, C.; Sauro, U.; et al. La Grotta di Carburangeli – ricostruzione climatica dell' Olocene per la piana costiera della Sicilia nord-occidentale. *Studi Trent. Sci. Nat. Acta Geol.* **2003**, *80*, 153–167.

82. Stoykova, D.; Shopov, Y.; Sauro, U.; Borsato, A.; Cucchi, F.; Forti, P. High-Resolution Climate Proxy Records for the Last 2000 Years from a Speleothem from Savi Cave, Trieste, NE Italy. *Studi Trent. Sci. Nat. Acta Geol.* **2003**, *80*, 169–173.

83. Genty, D.; Massault, M.; Gilmour, M.; Baker, A.; Verheyden, S.; Kepens, E. Calculations of past dead carbon proportion and variability by the comparison of AMS 14C and TIMS U/Th ages on two Holocene stalagmites. *Radiocarbon* **1999**, *41*, 251–270. [CrossRef]

84. Genty, D.; Vokal, B.; Obelic, B.; Massault, M. Bomb 14 C time history recorded in two modern stalagmites —Importance for soil organic matter dynamics and bomb 14 C distribution over continents. *Earth Planet. Sci. Lett.* **1998**, *160*, 795–809. [CrossRef]

85. Vansteenberge, S.; Verheyden, S.; Cheng, H.; Edwards, L.R.; Keppens, E.; Claeys, P. Paleoclimate in continental northwestern Europe during the Eemian and early Weichselian (125-97 ka): Insights from a Belgian speleothem. *Clim. Past* **2016**, *12*, 1445–1458. [CrossRef]

86. Van Rampelbergh, M.; Verheyden, S.; Allan, M.; Quinif, Y.; Cheng, H.; Edwards, L.R.; Keppens, E.; Claeys, P. A 500-year seasonally resolved $\delta^{18}O$ and $\delta^{13}C$, layer thickness and calcite aspect record from a speleothem deposited in the Han-sur-Lesse cave, Belgium. *Clim. Past* **2015**, *11*, 789–802. [CrossRef]

87. Moseley, G.E.; Spötl, C.; Svensson, A.; Cheng, H.; Brandstätter, S.; Edwards, R.L. Multi-speleothem record reveals tightly coupled climate between central europe and greenland during marine isotope stage 3. *Geology* **2014**, *42*, 1043–1046. [CrossRef]

88. Moseley, G.E.; Spötl, C.; Cheng, H.; Boch, R.; Min, A.; Edwards, R.L. Termination-II interstadial/stadial climate change recorded in two stalagmites from the north European Alps. *Quat. Sci. Rev.* **2015**, *127*, 229–239. [CrossRef]

89. Wurth, G.; Niggemann, S.; Richter, D.K.; Mangini, A. The Younger Dryas and Holocene climate record of a stalagmite from Hölloch Cave(Bavarian Alps, Germany. *J. Quat. Sci.* **2004**, *19*, 291–298. [CrossRef]

90. Spötl, C.; Mangini, A. U/Th age constraints on the absence of ice in the central Inn Valley (eastern Alps, Austria) during Marine Isotope Stages 5c to 5a. *Quat. Res.* **2006**, *66*, 167–175.

91. Verheyden, S.; Keppens, E.; van Strydonck, M.; Quinif, Y. The 8.2 ka event: its it registered in Belgian speleothems? *Speleogenesis Evolution Karst Aquifers* **2012**, *12*.

92. Domínguez-Villar, D.; Wang, X.; Krklec, K.; Cheng, H.; Edwards, R.L. The control of the tropical North Atlantic on Holocene millennial climate oscillations. *Geology* **2017**, *45*, 303–306. [CrossRef]

93. Boch, R.; Spötl, C.; Kramers, J. High-resolution isotope records of early Holocene rapid climate change from two coeval stalagmites of Katerloch Cave, Austria. *Quat. Sci. Rev.* **2009**, *28*, 2527–2538. [CrossRef]

94. Boch, R.; Spötl, C.; Frisia, S. Origin and palaeoenvironmental significance of lamination in stalagmites from Katerloch Cave, Austria. *Sedimentology* **2011**, *58*, 508–531. [CrossRef]

95. Boch, R.; Spötl, C. Reconstructing palaeoprecipitation from an active cave flowstone. *J. Quat. Sci.* **2011**, *26*, 675–678. [CrossRef]

96. Spötl, C.; Mangini, A.; Richards, D.A. Chronology and paleoenvironment of Marine Isotope Stage 3 from two high-elevation speleothems, Austrian Alps. *Quat. Sci. Rev.* **2006**, *25*, 1127–1136.

97. Sundqvist, H.S.; Holmgren, K.; Moberg, A.; Spötl, C.; Mangini, A. Stable isotopes in a stalagmite from NW Sweden document environmental changes over the past 4000 years. *Boreas* **2010**, *39*, 77–86. [CrossRef]

98. Sundqvist, H.S.; Holmgren, K.; Lauritzen, S.-E. Stable isotope variations in stalagmites from northwestern Sweden document climate and environmental changes during the early Holocene. *Holocene* **2007**, *17*, 259–267. [CrossRef]

99. Baldini, L.; Mcdermott, F.; Baldini, J.U.L.; Arias, P.; Cueto, M.; Fairchild, I.J.; Hoffmann, D.L.; Mattey, D.P.; Müller, W.; Constantin Nita, D.; Ontanon, R.; Garcia-Monco, C.; Richards, D.A. Regional temperature, atmospheric circulation, and sea-ice variability within the Younger Dryas Event constrained using a speleothem from northern Iberia. *Earth Planet. Sci. Lett.* **2015**, *419*, 101–110. [CrossRef]

100. Comas-Bru, L.; McDermott, F.; Fleitmann, D. A 1,000 Year Annually Resolved Record of Speleothem δ18O from Northern Spain; a potential new proxy for North Atlantic Oscillation (NAO) index reconstruction. In *Geophysical Research Abstract*; EGU General Assembly: Viena, Austria, April 2012.

101. Atkinson, T.C.; Hopley, P.J. Speleothems and Palaeoclimates. In *Caves and Karst of the Yorkshire Dales*; Wiley-Blackwell: Buxton, UK, 2013; pp. 181–186.

102. Atkinson, T.; Hoffmann, D.L. Unpublished dataset.

103. Linge, H.; Baker, A.; Andersson, C.; Lauritzen, S.E. Variability in luminescent lamination and initial230Th/232Th activity ratios in a late Holocene stalagmite from northern Norway. *Quat. Geochronol.* **2009**, *4*, 181–192. [CrossRef]

104. Luetscher, M.; Hoffmann, D.L.; Frisia, S.; Spötl, C. Holocene glacier history from alpine speleothems, Milchbach cave, Switzerland. *Earth Planet. Sci. Lett.* **2011**, *302*, 95–106. [CrossRef]

105. Munoz, A.; Bartolome, M.; Munoz, A.; Sancho, C.; Moreno, A.; Hellstrom, J.C.; Osácar, Mª.C.; Cacho, I. Solar influence and hydrological variability during the Holocene from a speleothem annual record (Molinos Cave, NE Spain). *Terra Nova* **2015**, *27*, 300–311. [CrossRef]

106. Mattey, D.P.; Fairchild, I.A.N.J.; Atkinson, T.I.M.C.; Latin, J.; Ainsworth, M.; Durell, R. Seasonal microclimate control of calcite fabrics, stable isotopes and trace elements in modern speleothem from St Michaels Cave, Gibraltar. In *Tufas and Speleothems: Unravelling the Microbial and Physical Controls*; Pedley, H.M., Rogerson, M., Eds.; Geological Society of London: London, UK, 2010; pp. 323–344.

107. Linge, H.; Lauritzen, S.E.; Andersson, C.; Hansen, J.K.; Skoglund, R.O.; Sundqvist, H.S. Stable isotope records for the last 10 000 years from Okshola cave (Fauske, northern Norway) and regional comparisons. *Clim. Past* **2009**, *5*, 667–682. [CrossRef]

108. Verheyden, S.; Keppens, E.; Quinif, Y.; Cheng, H.; Edwards, L. Late-glacial and Holocene climate reconstruction as inferred from a stalagmite—Grotte du Pere Noel, Han-sur-Lesse, Belgium. *Geologica Belgica* **2014**, *17*, 83–89.

109. Moreno, A.; Stoll, H.; Jiménez-Sánchez, M.; Cacho, I.; Valero-Garcés, B.; Ito, E.; Edwards, R.L. A speleothem record of glacial (25–11.6 kyr BP) rapid climatic changes from northern Iberian Peninsula. *Glob. Planet. Chang.* **2010**, *71*, 218–231. [CrossRef]

110. Rudzka, D.; McDermott, F.; Baldini, L.M.; Fleitmann, D.; Moreno, A.; Stoll, H. The coupled d13C-radiocarbon systematics of three Late Glacial/early Holocene speleothems; insights into soil and cave processes at climatic transitions. *Geochim. Cosmochim. Acta* **2011**, *75*, 4321–4339. [CrossRef]

111. Daley, T.J.; Thomas, E.R.; Holmes, J.A.; Street-Perrott, F.A.; Chapman, M.R.; Tindall, J.C.; Valdes, P.J.; Loader, N.J.; Marshall, J.D.; Wolff, E.W.; et al. The 8200yr BP cold event in stable isotope records from the North Atlantic region. *Glob. Planet. Chang.* **2011**, *79*, 288–302. [CrossRef]

112. Häuselmann, A.D.; Fleitmann, D.; Cheng, H.; Tabersky, D.; Günther, D.; Edwards, R.L. Timing and nature of the penultimate deglaciation in a high alpine stalagmite from Switzerland. *Quat. Sci. Rev.* **2015**, *126*, 264–275.

113. Bartolomé, M.; Moreno, A.; Sancho, C.; Stoll, H.M.; Cacho, I.; Spötl, C.; Belmonte, Á.; Edwards, R.L.; Cheng, H.; Hellstrom, J.C. Hydrological change in Southern Europe responding to increasing North Atlantic overturning during Greenland Stadial 1. *Proc. Natl. Acad. Sci. USA* **2015**, *112*, 6568–6572. [CrossRef] [PubMed]

114. Luetscher, M.; Boch, R.; Sodemann, H.; Spötl, C.; Cheng, H.; Edwards, R.L.; Frisia, S.; Hof, F.; Müller, W. North Atlantic storm track changes during the Last Glacial Maximum recorded by Alpine speleothems. *Nat. Commun.* **2015**, *6*, 6344. [CrossRef] [PubMed]

115. Berstad, I. *Uranseriedatering og Stabilisotopanalyse av Speleothe- mer fra Søylegrotta, Mo i Rana*; University of Bergen: Bergen, Norway, 1998.

116. Fohlmeister, J.; Vollweiler, N.; Spötl, C.; Mangini, A. COMNISPA II: Update of a mid-European isotope climate record, 11 ka to present. *Holocene* **2012**. [CrossRef]

117. Spötl, C.; Scholz, D.; Mangini, A. A terrestrial U/Th-dated stable isotope record of the Penultimate Interglacial. *Earth Planet. Sci. Lett.* **2008**, *276*, 283–292. [CrossRef]

118. Cliff, R.A.; Spötl, C.; Mangini, A. U-Pb dating of speleothems from Spannagel Cave, Austrian Alps: A high resolution comparison with U-series ages. *Quat. Geochronol.* **2010**, *5*, 452–458. [CrossRef]

119. Spötl, C.; Mangini, A. Speleothems and paleoglaciers. *Earth Planet. Sci. Lett.* **2007**, *254*, 323–331. [CrossRef]

120. Holzkämper, S.; Mangini, A.; Spötl, C.; Mudelsee, M. Timing and progression of the Last Interglacial derived from a high alpine stalagmite. *Geophys. Res. Lett.* **2004**, *31*. [CrossRef]

121. Mangini, A.; Spötl, C.; Verdes, P. Reconstruction of temperature in the Central Alps during the past 2000 yr from a d18O stalagmite record. *Earth Planet. Sci. Lett.* **2005**, *235*, 741–751. [CrossRef]

122. Spötl, C.; Mangini, A.; Frank, N.; Eichstädter, R.; Burns, S.J. Start of the last interglacial period at 135 ka: Evidence from a high Alpine speleothem. *Geology* **2002**, *30*, 815–818. [CrossRef]

123. Baker, A.; Wilson, R.; Fairchild, I.J.; Franke, J.; Spötl, C.; Mattey, D.; Trouet, V.; Fuller, L. High resolution δ18O and δ13C records from an annually laminated Scottish stalagmite and relationship with last millennium climate. *Glob. Planet. Chang.* **2011**, *79*, 303–311. [CrossRef]

124. Baker, A.; Bradley, C.; Phipps, S.J.; Fischer, M.; Fairchild, I.J.; Fuller, L.; Spaptl, C.; Azcurra, C. Millennial-length forward models and pseudoproxies of stalagmite δ18O: An example from NW Scotland. *Clim. Past* **2012**, *8*, 1153–1167. [CrossRef]

125. Genty, D. Unpublished dataset.

126. Genty, D.; Blamart, D.; Ouahdi, R.; Gilmour, M.; Baker, A.; Jouzel, J.; Van-Exter, S. Precise dating of Dansgaard-Oeschger climate oscillations in western Europe from stalagmite data. *Nature* **2003**, *421*, 833–837. [CrossRef] [PubMed]

127. Genty, D.; Combourieu-Nebout, N.; Peyron, O.; Blamart, D.; Wainer, K.; Mansuri, F.; Ghaleb, B.; Isabello, L.; Dormoy, I.; von Grafenstein, U.; et al. Isotopic characterization of rapid climatic events during OIS3 and OIS4 in Villars Cave stalagmites (SW-France) and correlation with Atlantic and Mediterranean pollen records. *Quat. Sci. Rev.* **2010**, *29*, 2799–2820. [CrossRef]

128. Wainer, K.; Genty, D.; Blamart, D.; Hoffmann, D.; Couchoud, I. A new stage 3 millennial climatic variability record from a SW France speleothem. *Palaeogeogr. Palaeoclimatol. Palaeoecol.* **2009**, *271*, 130–139. [CrossRef]

129. Wainer, K.; Genty, D.; Blamart, D.; Daëron, M.; Bar-Matthews, M.; Vonhof, H.; Dublyansky, Y.; Pons-Branchu, E.; Thomas, L.; van Calsteren, P.; et al. Speleothem record of the last 180 ka in Villars cave (SW France): Investigation of a large δ18O shift between MIS6 and MIS5. *Quat. Sci. Rev.* **2011**, *30*, 130–146. [CrossRef]

130. Labuhn, I.; Genty, D.; Vonhof, H.; Bourdin, C.; Blamart, D.; Douville, E.; Ruan, J.; Cheng, H.; Edwards, R.L.; Pons-Branchu, E.; et al. A high-resolution fluid inclusion δ18O record from a stalagmite in SW France: Modern calibration and comparison with multiple proxies. *Quat. Sci. Rev.* **2015**, *110*, 152–165. [CrossRef]

131. Cheng, H.; Lawrence Edwards, R.; Shen, C.C.; Polyak, V.J.; Asmerom, Y.; Woodhead, J.; Hellstrom, J.; Wang, Y.; Kong, X.; Spötl, C.; et al. Improvements in 230Th dating, 230Th and 234U half-life values, and U-Th isotopic measurements by multi-collector inductively coupled plasma mass spectrometry. *Earth Planet. Sci. Lett.* **2013**, *371–372*, 82–91. [CrossRef]

132. Cheng, H.; Edwards, R.L.; Hoff, J.; Gallup, C.D.; Richards, D.A.; Asmerom, Y. The half-lives of uranium-234 and thorium-230. *Chem. Geol.* **2000**, *169*, 17–33. [CrossRef]

133. Edwards, R.L.; Chen, J.H.; Wasserburg, G.J. U-238-U-234-Th-230-Th-232 systematics and the precise measurement of time over the past 500,000 years. *Earth Planet. Sci. Lett.* **1987**, *81*, 175–192. [CrossRef]

134. Baker, A.; Hellstrom, J.C.; Kelly, B.F.J.; Mariethoz, G.; Trouet, V. A composite annual-resolution stalagmite record of North Atlantic climate over the last three millennia. *Sci. Rep.* **2015**, *5*. [CrossRef] [PubMed]

135. Hua, Q.; McDonald, J.; Redwood, D.; Drysdale, R.; Lee, S.; Fallon, S.; Hellstrom, J. Robust chronological reconstruction for young speleothems using radiocarbon. *Quat. Geochronol.* **2012**, *14*, 67–80. [CrossRef]

136. Shen, C.-C.; Lin, K.; Duan, W.; Jiang, X.; Partin, J.W.; Edwards, R.L.; Cheng, H.; Tan, M. Testing the annual nature of speleothem banding. *Sci. Rep.* **2013**, *3*. [CrossRef] [PubMed]

137. Domínguez-Villar, D.; Baker, A.; Fairchild, I.J.; Edwards, R.L. A method to anchor floating chronologies in annually laminated speleothems with U-Th dates. *Quat. Geochronol.* **2012**, *14*, 57–66. [CrossRef]

138. Scholz, D.; Hoffmann, D.L. StalAge—An algorithm designed for construction of speleothem age models. *Quat. Geochronol.* **2011**, *6*, 369–382. [CrossRef]

139. Bronk Ramsey, C. Deposition models for chronological records. *Quat. Sci. Rev.* **2008**, *27*, 42–60. [CrossRef]

140. Bajo, P.; Hellstrom, J.; Frisia, S.; Drysdale, R.; Black, J.; Woodhead, J.; Borsato, A.; Zanchetta, G.; Wallace, M.W.; Regattieri, E.; et al. "Cryptic" diagenesis and its implications for speleothem geochronologies. *Quat. Sci. Rev.* **2016**, *148*, 17–28. [CrossRef]

141. Railsback, L.B.; Dabous, A.A.; Osmond, J.K.; Fleisher, C.J. Petrographic and geochemical screening of speleothems for U-series dating: An example from recrystallized speleothems from Wadi Sannur Cavern, Egypt. *J. Cave Karst Stud.* **2002**, *64*, 108–116.

142. De Waele, J.; D'Angeli, I.M.; Bontognali, T.; Tuccimei, P.; Scholz, D.; Jochum, K.P.; Columbu, A.; Bernasconi, S.M.; Fornós, J.J.; Grau González, E.R.; et al. Speleothems in a north Cuban cave register sea level changes and Pleistocene uplift rates. *Earth Surf. Process. Landf.* **2018**, *43*, 2313–2326. [CrossRef]

143. Scholz, D.; Tolzmann, J.; Hoffmann, D.L.; Jochum, K.P.; Spötl, C.; Riechelmann, D.F.C. Diagenesis of speleothems and its effect on the accuracy of 230Th/U-ages. *Chem. Geol.* **2014**, *387*, 74–86. [CrossRef]

144. Scholz, D.; Hoffmann, D.L.; Hellstrom, J.; Bronk Ramsey, C. A comparison of different methods for speleothem age modelling. *Quat. Geochronol.* **2012**, *14*, 94–104. [CrossRef]

145. van der Meulen, J.P.; Brandsma, T. Thermometer screen intercomparison in De Bilt (The Netherlands), Part I: Understanding the weather-dependent temperature differences. *Int. J. Climatol.* **2008**, *28*, 371–387. [CrossRef]

146. Parker, D.E.; Legg, T.P.; Folland, C.K. A new daily central England temperature series, 1772–1991. *Int. J. Climatol.* **1992**, *12*, 317–342. [CrossRef]

147. Moberg, A.; Bergström, H.; Ruiz Krigsman, J.; Svanered, O. Daily air temperature and pressure series for Stockholm (1756–1998). *Clim. Chang.* **2002**, *53*, 171–212. [CrossRef]

148. Fuller, L.; Baker, A.; Fairchild, I.J.; Spötl, C.; Marca-Bell, A.; Rowe, P.; Dennis, P.F. Isotope hydrology of dripwaters in a Scottish cave and implications for stalagmite palaeoclimate research. *Hydrol. Earth Syst. Sci.* **2008**, *12*, 1065–1074. [CrossRef]

149. Mischel, S.A.; Scholz, D.; Spötl, C. δ18O values of cave drip water: A promising proxy for the reconstruction of the North Atlantic Oscillation? *Clim. Dyn.* **2015**, *45*, 3035–3050. [CrossRef]

150. Perez-Mejias, C.; Moreno, A.; Sancho, C.; Bartolome, M.; Stoll, H.M.; Osacar, M.C.; Cacho, I.; Delgado-Huertas, A. Transference of isotopic signal from rainfall to dripwaters and farmed calcite in Mediterranean semi-arid karst. *Geochim. Cosmochim. Acta* **2018**, *243*, 66–98. [CrossRef]

151. Tan, M.; Baker, A.; Genty, D.; Smith, C.; Esper, J.; Cai, B. Applications of stalagmite laminae to paleoclimate reconstructions: Comparison with dendrochronology/climatology. *Quat. Sci. Rev.* **2006**, *25*, 2103–2117. [CrossRef]

152. Vaks, A.; Gutareva, O.S.; Breitenbach, S.F.M.; Avirmed, E.; Mason, A.J.; Thomas, A.L.; Osinzev, A.V.; Kononov, A.M.; Henderson, G.M. Speleothems Reveal 500,000-Year History of Siberian Permafrost. *Science* **2013**, *340*, 183–186. [CrossRef]

153. Columbu, A.; Chiarini, V.; De Waele, J.; Spötl, C.; Luetscher, M.; Hellstrom, J. Last glaciation 70 kyrs-long stalagmite palaeoclimate record from Southern Italy: Implication for Mediterranean climate during glacial shifts. In Proceedings of the Proceedings of SGI Conference 2018, Catania, Italy, 12–14 September 2018.

154. Dansgaard, W. Stable isotopes in precipitation. *Tellus* **1964**, *16*, 436–468. [CrossRef]

155. Moreno, A.; Sancho, C.; Bartolomé, M.; Oliva-Urcia, B.; Delgado-Huertas, A.; Estrela, M.J.; Corell, D.; López-Moreno, J.I.; Cacho, I. Climate controls on rainfall isotopes and their effects on cave drip water and speleothem growth: The case of Molinos cave (Teruel, NE Spain). *Clim. Dyn.* **2014**, *43*, 221–241. [CrossRef]

156. Dumitru, O.A.; Onac, B.P.; Polyak, V.J.; Wynn, J.G.; Asmerom, Y.; Fornós, J.J. Climate variability in the western Mediterranean between 121 and 67 ka derived from a Mallorcan speleothem record. *Palaeogeogr. Palaeoclimatol. Palaeoecol.* **2018**, *506*, 128–138. [CrossRef]

157. Laîné, A.; Kageyama, M.; Salas-Mélia, D.; Voldoire, A.; Rivièlre, G.; Ramstein, G.; Planton, S.; Tyteca, S.; Peterschmitt, J.Y. Northern hemisphere storm tracks during the last glacial maximum in the PMIP2 ocean-atmosphere coupled models: Energetic study, seasonal cycle, precipitation. *Clim. Dyn.* **2009**, *32*, 593–614. [CrossRef]

158. van Breukelen, M.R.; Vonhof, H.B.; Hellstrom, J.C.; Wester, W.C.G.; Kroon, D. Fossil dripwater in stalagmites reveals Holocene temperature and rainfall variation in Amazonia. *Earth Planet. Sci. Lett.* **2008**, *275*, 54–60. [CrossRef]

159. Affolter, S.; Häuselmann, A.D.; Fleitmann, D.; Häuselmann, P.; Leuenberger, M. Triple isotope (δD, δ17O, δ18O) study on precipitation, drip water and speleothem fluid inclusions for a Western Central European cave (NW Switzerland). *Quat. Sci. Rev.* **2015**, *127*, 73–89. [CrossRef]

160. Affolter, S.; Fleitmann, D.; Leuenberger, M. New online method for water isotope analysis of speleothem fluid inclusions using laser absorption spectroscopy (WS-CRDS). *Clim. Past* **2014**, *10*, 1291–1304. [CrossRef]

161. Dassié, E.P.; Genty, D.; Noret, A.; Mangenot, X.; Massault, M.; Lebas, N.; Duhamel, M.; Bonifacie, M.; Gasparrini, M.; Minster, B.; et al. A Newly Designed Analytical Line to Examine Fluid Inclusion Isotopic Compositions in a Variety of Carbonate Samples. *Geochem. Geophys. Geosyst.* **2018**. [CrossRef]

162. Bowen, G.J.; Revenaugh, J. Interpolating the isotopic composition of modern meteoric precipitation. *Water Resour. Res.* **2003**, *39*, 1–13. [CrossRef]

163. Bowen, G.J. Waterisotopes Database. 2018. Available online: www.waterisotopes.org. (accessed on 14 June 2018).

164. Wackerbarth, A.; Langebroek, P.M.; Werner, M.; Lohmann, G.; Riechelmann, S.; Borsato, A.; Mangini, A. Simulated oxygen isotopes in cave drip water and speleothem calcite in European caves. *Clim. Past* **2012**, *8*, 1781–1799. [CrossRef]

165. Wirth, S.B.; Glur, L.; Gilli, A.; Anselmetti, F.S. Holocene flood frequency across the Central Alps—Solar forcing and evidence for variations in North Atlantic atmospheric circulation. *Quat. Sci. Rev.* **2013**, *80*, 112–128. [CrossRef]

166. Rasmussen, S.O.; Bigler, M.; Blockley, S.P.; Blunier, T.; Buchardt, S.L.; Clausen, H.B.; Cvijanovic, I.; Dahl-Jensen, D.; Johnsen, S.J.; Fischer, H.; et al. A stratigraphic framework for abrupt climatic changes during the Last Glacial period based on three synchronized Greenland ice-core records: Refining and extending the INTIMATE event stratigraphy. *Quat. Sci. Rev.* **2014**, *106*, 14–28. [CrossRef]

167. Wolff, E.W.; Chappellaz, J.; Blunier, T.; Rasmussen, S.O.; Svensson, A. Millennial-scale variability during the last glacial: The ice core record. *Quat. Sci. Rev.* **2010**, *29*, 2828–2838. [CrossRef]

168. NGRIP Project Members High-resolution record of Northern Hemisphere climate extending into the last interglacial period. *Nature* **2004**, *431*, 147–151. [CrossRef] [PubMed]

169. Svensson, A.; Andersen, K.K.; Bigler, M.; Clausen, H.B.; Dahl-Jensen, D.; Davies, S.M.; Johnsen, S.J.; Muscheler, R.; Parrenin, F.; Rasmussen, S.O.; et al. A 60,000 year Greenland stratigraphic ice core chronology. *Clim. Past* **2008**, *4*, 47–57. [CrossRef]

170. Rehfeld, K.; Münch, T.; Ho, S.L.; Laepple, T. Global patterns of declining temperature variability from the Last Glacial Maximum to the Holocene. *Nature* **2018**, *554*, 356–359. [CrossRef] [PubMed]

171. Rohling, E.J.; Pälike, H. Centennial-scale climate cooling with a sudden cold event around 8,200 years ago. *Nature* **2005**, *434*, 975–979. [CrossRef]

172. Sigl, M.; Winstrup, M.; Mcconnell, J.R.; Welten, K.C.; Plunkett, G.; Ludlow, F.; Büntgen, U.; Caffee, M.; Chellman, N.; Dahl-Jensen, D.; et al. Timing and climate forcing of volcanic eruptions for the past 2,500 years. *Nature* **2015**, *523*, 543–549. [CrossRef]

173. Steinhilber, F.; Beer, J.; Fröhlich, C. Total solar irradiance during the Holocene. *Geophys. Res. Lett.* **2009**, *36*, 1–5. [CrossRef]

174. Köhler, P.; Nehrbass-Ahles, C.; Schmitt, J.; Stocker, T.F.; Fischer, H. A 156 kyr smoothed history of the atmospheric greenhouse gases CO_2, CH_4, and N_2O and their radiative forcing. *Earth Syst. Sci. Data* **2017**, *9*, 363–387. [CrossRef]

175. PAGES 2k Consortium Continental-scale temperature variability during the past two millennia. *Nat. Geosci.* **2013**, *6*, 339–346. [CrossRef]

176. Mann, M.E.; Zhang, Z.; Rutherford, S.; Bradley, R.S.; Hughes, M.K.; Shindell, D.; Ammann, C.; Faluvegi, G.; Ni, F. Global signatures and dynamical origins of the Little Ice Age and Medieval Climate Anomaly. *Science* **2009**, *326*, 1256–1260. [CrossRef] [PubMed]

177. Büntgen, U.; Myglan, V.S.; Ljungqvist, F.C.; Mccormick, M.; Di Cosmo, N.; Sigl, M.; Jungclaus, J.; Wagner, S.; Krusic, P.J.; Esper, J.; et al. Cooling and societal change during the Late Antique Little Ice Age from 536 to around 660 AD. *Nat. Geosci.* **2016**, *9*, 231–236. [CrossRef]

178. Cheng, H.; Edwards, R.L.; Sinha, A.; Spötl, C.; Yi, L.; Chen, S.; Kelly, M.; Kathayat, G.; Wang, X.; Li, X.; et al. The Asian monsoon over the past 640,000 years and ice age terminations. *Nature* **2016**, *534*, 640–646. [CrossRef] [PubMed]

179. Stoll, H.; Perez, C.; Cacho, I.; Moreno, A.; Iglesias, M.; Edwards, R.L. Chronlogy for deglaciation during Termination II from stalagmites in NW Spain. In Proceedings of the Geophysical Research Abstracts—EGU2018, Vienna, Austria, 7–12 April 2018.